Journal of the Meteorological Society of Japan, Vol. 87, No. 3, pp. 423–457, 2009.
DOI:10.2151/jmsj.87.423

Mesoscale Development and Along-Frontal Variation of a Meiyu/Baiu Front and Precipitation Observed in the Downstream Region of the Yangtze River

Biao GENG, Hiroyuki YAMADA, Krishnareddigari Krishna REDDY

Institute of Observational Research for Global Change, JAMSTEC, Yokosuka, Japan

Hiroshi UYEDA

Hydrospheric Atmospheric Research Center, Nagoya University, Nagoya, Japan

and

Yasushi FUJIYOSHI

Institute of Low Temperature Science, Hokkaido University, Sapporo, Japan

(Manuscript received 21 May 2007, in final form 26 February 2009)

Abstract

This paper has investigated the mesoscale structure and evolution of a Meiyu/Baiu front and precipitation along the front observed in the downstream region of the Yangtze River on 21 June 2002 by using data from intensive observations of upper-air, surface, and five Doppler radars, as well as GMS IR and GANAL re-analysis data. It is found that the front collocated with a large-scale wind shear line. The frontal zone was characterized by a subsynoptic-scale low-level jet (LLJ) to the south and a thermally direct circulation in the middle troposphere south of the surface front.

The front evolved from an inactive front with little convection along it to an intensive one triggering a strong meso-α-scale rainband. The front initially intensified mainly in association with the divergence related to the evaporative cooling of precipitation systems north of the front and further developed when strong convection evolved along the front. The meso-α-scale rainband triggered by the front was composed of several meso-β-scale convective systems. Meso-β-scale convective systems were narrow and consolidated in the western part, but wide and weak in the eastern part of the downstream region of the Yangtze River.

Three-dimensional kinematic and reflectivity structures of two meso-β-scale convective systems, where one was in the western part and the other was in the eastern part, have been examined comprehensively. In the western part, the convective system evolved in a quasi-steady state and was characterized by a deep and strong convective cell just north of the front and limited stratiform precipitation further north of the front. The orientation of the LLJ to the front was at a sharp angle. The primary updraft triggered by the front sloped largely northward in the lower troposphere and became nearly upright and strong from the middle troposphere. In the eastern part, on the other hand, the convective system changed remarkably with time and was featured by multiple shallow and weak convective cells across the front and extended stratiform precipitation both south and north of convective cells. The LLJ that oriented nearly normal to the front overran the front at lower levels and penetrated far to the north of the front.

Corresponding author: Biao Geng, Institute of Observational Research for Global Change, Japan Agency for Marine-Earth Science and Technology, 2-15 Natsushima, Yokosuka, 237-0061, Japan.
E-mail: bgeng@jamstec.go.jp

It appears that the variable structure and evolution of the LLJ would have a great impact on the development of distinct convective systems in the downstream region of the Yangtze River. The mesoscale along-frontal variability of the Meiyu/Baiu frontal zone appears to be responsible for distinct modes of convective organization along the front in a limited distance.

1. Introduction

The Meiyu/Baiu front is a quasi-stationary frontal system that develops and extends from the inland of China to Japan. As the Meiyu/Baiu front is the most important rain-producing system in these regions from late spring to early summer and has a great impact on regional-scale water cycles and climates, the structure and evolution of the Meiyu/Baiu front and associated precipitation systems have been one of the most important research topics.

Many studies have illustrated large scale and mesoscale features of the active Meiyu/Baiu front triggering vigorous convection (e.g., Ding 1992; Ninomiya and Akiyama 1992; Chen 2004). These studies indicated that strong convection forms over the low-level convergence zone associated with the front. It also takes place with the presence of a mid-tropospheric shortwave trough and mid- and upper-tropospheric divergence over the frontal zone. The lower- and mid-tropospheric atmosphere south of the front is usually potentially unstable. On the other hand, there often exist inactive phases of the Meiyu/Baiu front (Akiyama 1990). During inactive phases, the Meiyu/Baiu frontal disturbances are weak and relatively dry Meiyu/Baiu fronts are observed (e.g., Chen et al. 1989; Chen and Hui 1990; 1992). For the dry Meiyu/Baiu front, only weak or little convection is found over the front. It is apparently important to know how a relatively weak and inactive Meiyu/Baiu front develops into the strong and active one inducing the formation of intense convection. However, very few observational studies have documented mesoscale developing processes related to the activation of the Meiyu/Baiu front.

It is well known that the synoptic-scale structure and dynamics of the Meiyu/Baiu front are largely different over distinct geographic locations (e.g., Chen and Chang 1980; Kato 1985; Ninomiya and Muraki 1986). Previous studies indicated that the Meiyu/Baiu front is characterized by a strong horizontal temperature gradient near Japan, whereas it is characterized by a weak horizontal temperature gradient and a strong lower-tropospheric horizontal wind shear over China. Such a large-scale along-frontal variation in the frontal structure accounts for the difference in cloud features between the western and the eastern Meiyu/Baiu front (Akiyama 1989; Akiyama 1990). On the other hand, Ninomiya and Akiyama (1992) emphasized the multi-scale features of the Meiyu/Baiu front. They pointed out that synoptic-scale and mesoscale motions were interacting with each other around the Meiyu/Baiu frontal zone. Their study implies that the Meiyu/Baiu front could evolve with a distinct mesoscale structure along the front. In contrast to the large-scale variability along the Meiyu/Baiu front, much less attention has been paid to the mesoscale along-frontal variability of the Meiyu/Baiu frontal zone.

Heavy rainfall is often induced by the Meiyu/Baiu front both in China and Japan. While favorable large-scale conditions take place over a much larger area, the heavy rainfall during the Meiyu/Baiu season often occurs within a small region of the area. For example, many studies have emphasized the close relationship between a low-level jet (LLJ) and the heavy rainfall over the Meiyu/Baiu front (e.g., Matsumoto et al. 1971; Ninomiya and Akiyama 1974; Ogura et al. 1985; Ninomiya 2000), because the LLJ induces large-scale convergence on its northern side and transports warm and moist air from the south at low levels (Ninomiya and Akiyama 1992). The LLJ usually refers to low-level winds south of the front with their speeds greater than 12 m s^{-1} and it is frequently located at altitudes of 1.5~3 km (Ding 1992). Some other studies, however, pointed out that the LLJ sometimes only induces a heavy rainfall in a limited region and fails to produce it in the neighboring region along the Meiyu/Baiu front (e.g., Chen and Li 1995; Li et al. 1997). Such a situation has caused the forecast for the heavy rainfall in some places based on the presence of the LLJ and the expected frontal passage to be wrong. Nevertheless, very few studies have analyzed variable effects of the LLJ on the distinct convective organization along the Meiyu/Baiu front in a limited region.

The internal structure of the Meiyu/Baiu front and mesoscale convective systems developing during the Meiyu/Baiu seasons have been studied for

a long time by using Doppler radar observation in Japan (e.g., Ishihara et al. 1995; Takahashi et al. 1996; Moteki et al. 2004), Korea (e.g., Kim and Lee 2006), China (e.g., Yamada et al. 2003; Geng et al. 2004), and Taiwan (e.g., Trier et al. 1990; Ray et al. 1991; Lin et al. 1992). During TAMEX (Taiwan Area Mesoscale Experiment), aircraft observations were also conducted to investigate the Meiyu/Baiu frontal convective systems (e.g., Jorgensen and LeMone 1989; Jorgensen et al. 1991). Most convective systems during the Meiyu/Baiu season possess linear structures. One interesting finding from previous studies is that strong convective systems often occur over a shallow Meiyu/Baiu front with a depth of 0.5~1.0 km (e.g., Trier et al. 1990; Geng et al. 2004). In a review of past researches on the Meiyu/Baiu front, Chen (2004) pointed out that the convective updrafts and cores observed in the Meiyu/Baiu front were comparable in size and strength with those measured in GATE (Global Atmospheric Research Program Atlantic Tropical Experiment) and hurricanes but much weaker than those measured in the Continental Thunderstorm Project. However, although previous studies have investigated various aspects of the internal structure and evolution of the Meiyu/Baiu front and mesoscale convective systems developing around the front, there are no studies that have used the Doppler radar observation to compare various convective systems that occurred along the same Meiyu/Baiu front within several hundred kilometers. Consequently, distinct convective organization along the Meiyu/Baiu front associated with the mesoscale along-frontal variation of the Meiyu/Baiu frontal zone has not been analyzed yet from the Doppler radar observation.

On 21 June 2002, a Meiyu/Baiu front was observed in the downstream region of the Yangtze River. This case was interesting because the front developed from a weak and dry front into a vigorous one inducing a strong convective rainband, with different frontal and precipitation structures in the western part from those in the eastern part of the downstream region of the Yangtze River. The purpose of this paper is to investigate the variable along-frontal structure and the evolution of the frontal zone and mesoscale convective systems. The analyzed results are used to discuss and illustrate processes related to the distinct mesoscale development of the front and convective systems along the front in the downstream region of the Yangtze River.

This paper is organized as follows. Section 2 will present a description of the data and analysis method used in this study. In section 3, a large scale overview and ambient atmospheric stratifications are provided. The structure and evolution of the surface and upper-air frontal zone are described in sections 4 and 5, respectively, by using surface and upper-air observations. In section 6, Doppler radar observations are used to examine the fine structure and evolution of the front and convective systems along the front. A discussion will be presented in section 7, followed by summary and conclusions in section 8.

2. Data and analysis method

During the Meiyu/Baiu season of 2002, intensive observations were conducted in the downstream region of the Yangtze River. In addition to routine observations, special upper-air, surface, as well as Doppler radar observations have also been conducted during the intensive observational period. Data employed in this study were from intensive upper-air, surface, and Doppler radar observations. Also, synoptic weather charts and GANAL (Global Objective Analysis) data from the Japan Meteorological Agency and satellite infrared images from the Weather Satellite Image Archive, Kochi University were used. Figure 1 shows geographical characteristics around the Yangtze River. The locations of radiosonde stations and Doppler radars are also shown in Fig. 1. The section of the front observed in the downstream region of the Yangtze River from about 117°E to 122°E is the main target of this paper. According to characteristics of the front and convective activities along the front, this section could be divided into two parts approximately separated by 119.5°E. Hereafter, these two parts will be referred to as the western part and the eastern part of the downstream region of the Yangtze River, respectively.

Routine upper-air sounding data were at 12-h intervals. In fifteen sounding stations that cover the middle and downstream regions of the Yangtze River (see filled black circles in Fig. 1), upper-air sounding observations were conducted at 6-h intervals. In order to make mesoscale analyses, the method shown by Chen and Li (1995) in processing TAMEX data has been used to interpolate upper-air sounding data into grids at constant pressure surfaces from the 1000-hPa level to the 100-hPa level. Like Chen and Li (1995), the horizontal interval was 80 km and the vertical interval was 50 hPa.

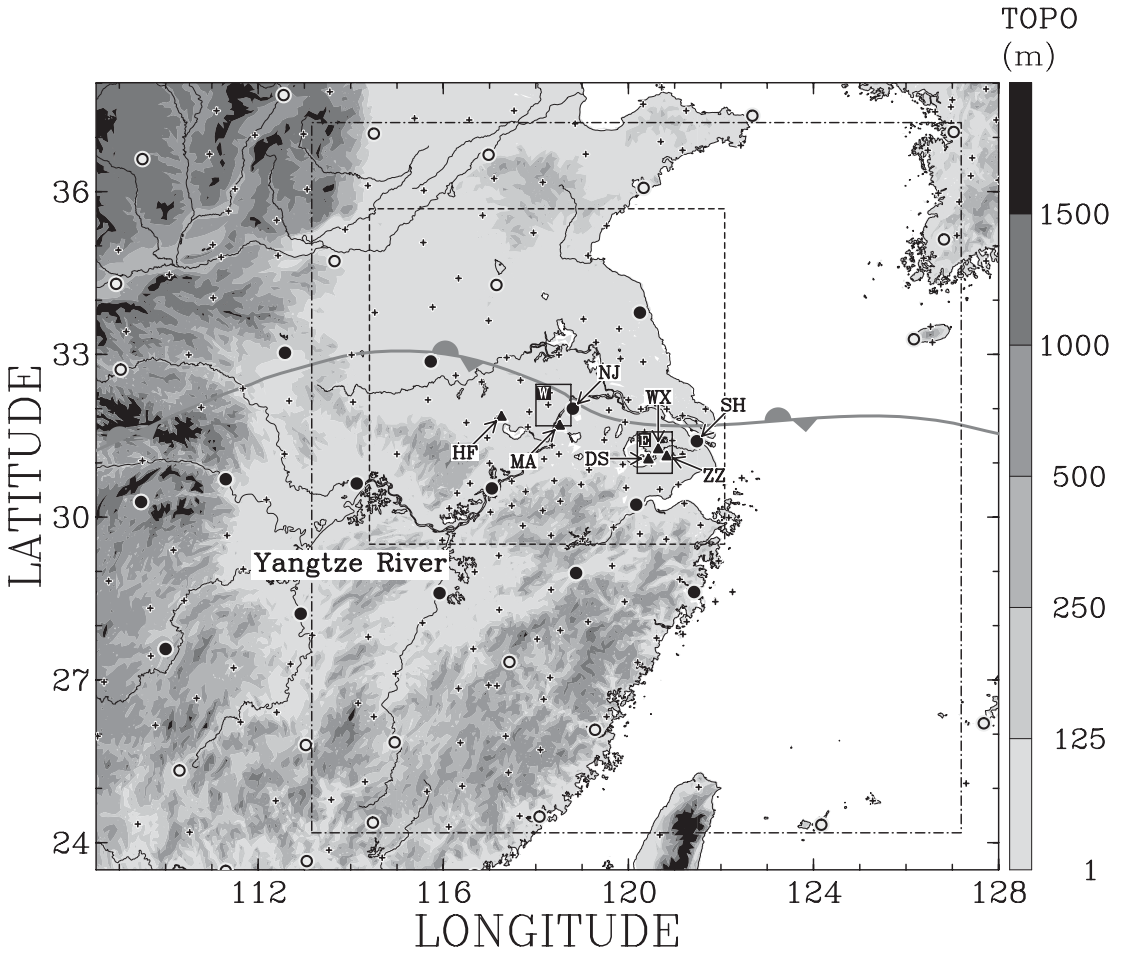

Fig. 1. Geographic map of the Yangtze River. Doppler radar positions (▲), rawinsonde stations (○ for 12-h interval and ● for 6-h interval) and surface stations (+) are shown. Doppler radars are named after the curt names of their locations, with HF being Hefei, MA being Maanshan, DS being Dongshan, WX being Wuxian, ZZ being Zhouzhuang. Boxes with dot-dashed and dashed lines represent the upper-air and surface analysis domains, respectively. The box labeled W indicates the dual-Doppler-radar analysis domain for the HF and MA radars and the box labeled E indicates the triple-Doppler-radar analysis domain for the DS, WX, and ZZ radars. NJ (Nanjing) and SH (Shanghai) indicate the rawinsonde stations where observational data are used to constitute skew-T log p diagrams in Fig. 4. Also shown is the location of the Meiyu/Baiu front for 0200 LST 21 June 2002.

The successive corrections technique developed by Cressman (1959) was used for the interpolation of upper-air data, with GANAL data ($1.25° \times 1.25°$) being used as initial guess fields. Then, the vertical p velocity was computed from variational integration of the continuity equation (O'Brien 1970). Surface data, which were at 3-h intervals, were objectively interpolated into grids of 40 km $\times$ 40 km by using Barnes' objective analysis scheme (Barnes 1964).

Data from five Doppler radars were used to analyze the internal structure of the front and convective systems. As shown in Fig. 1, the HF and MA radars were located in the western part of the downstream region of the Yangtze River. The HF radar was an S-band Doppler radar and the MA radar was a C-band Doppler radar. They were both operational radars of Chinese Meteorological Administration. Three X-band Doppler radars, the DS, WX, and ZZ radars, were brought from Japan and installed in the eastern part of the downstream region of the Yangtze River.

All Doppler radars performed volume scans at six-minute intervals. Volume scans from the HF and MA radars were used to retrieve three-dimensional reflectivity and wind fields in the domain labeled W, while volume scans from the DS, WX, and ZZ radars were used to retrieve three-dimensional reflectivity and wind fields in the domain labeled E as show in Fig. 1. Hereafter, these two domains will be referred to as the western and eastern domains for the Doppler radar analysis, respectively. The Meiyu/Baiu front has passed through both the western and eastern domains. Evidently, the Doppler radar analysis could reveal characteristics of the front and associated precipitation both in the western and eastern parts of the downstream region of the Yangtze River.

Doppler radar data were processed as follows. The removal of noise and the correction of folded Doppler velocities were performed in radar coordinates. Radar data were then interpolated to Cartesian grids using a Cressman (1959) weighting scheme. The horizontal grid interval was 1 km and the vertical grid interval was 0.5 km. Horizontal and vertical air motions were calculated from radial velocities in Cartesian grids after effects of particle fall speeds estimated from the reflectivity (Biggerstaff and Houze 1991) were initially removed. All winds in this paper were ground relative. A variational method described by Gao et al. (1999) and Shimizu and Maesaka (2007) was employed for retrieving three dimensional winds. The parameter settings used in this study were the same as those used by Gao et al. (1999).

The accuracy of the vertical velocity derived from multiple-Doppler radar observations is worthy of concern. Vertical velocity is usually obtained by vertical integration of the mass continuity equation. After the removal of noise and the correction of folded Doppler velocities, error sources particularly important in the vertical wind computation come from boundary condition errors due to data voids in the lower or upper regions of the storm observed by Doppler radars (Ray et al. 1980). The variational method used in this study applies the mass continuity equation as a weak constraint, so that the explicit setting of boundary conditions for the vertical velocity and the explicit integration of the mass continuity equation are avoided. As a result, error accumulation in the vertical velocity has been reduced. Nevertheless, errors could still exist in the vertical velocity even though the variational method has been applied. As a result, the reasonability of the vertical velocity derived from this study has been judged carefully by citing previous observational and numerical studies. Furthermore, the main purpose of this study is to compare distinct convection developed in different parts of a Meiyu/Baiu front. Therefore, the value of the vertical velocity is discussed in this study in some sense more relatively.

3. Large scale overview and ambient atmospheric stratifications

Characteristics of large scale conditions in this case resembled those of a typical Meiyu/Baiu front (e.g., Ding 1992; Chen 2004). Surface weather maps for 0200 LST (= UTC + 8 h) and 0800 LST 21 June are shown in Fig. 2. An east-west-oriented Meiyu/Baiu front extended from the inland of China to Japan. In the downstream region of the Yangtze River, the front evolved between a high pressure cell centered in the Northeastern China and a subtropical high with its center being located to the south of Japan. The front also collocated with a trough extending eastward from a low pressure centered around (29°N, 104–105°E).

Figure 3 shows synoptic weather maps at 850 hPa and 500 hPa for 0800 LST 21 June. Figure 3a indicates that the frontal zone was characterized by an area of copious moisture (the dotted area in the figure) extended along the front. Meanwhile, a subsynoptic-scale ($\sim$ 2000 km) LLJ with wind speed greater than 12 m s^{-1} was observed south of the front at the 850-hPa level. Note that the LLJ collocated with warm and moist air. At the 500-hPa level (Fig. 3b), a low pressure existed around (43°N, 133°E). To the south of the low pressure, the horizontal gradient of geopotential height was intense and stronger northwesterly winds with their speeds greater than 20 m s^{-1} were found. It is evident that the front was associated with a large-scale wind shear and a confluent zone from the surface to the 500-hPa level.

Although extended cloud developed along the front, it is noted that convection along the front over the downstream region of the Yangtze River was inactive at 0200 LST (Fig. 2a). At this time, satellite infrared imagery indicated that few cold IR clouds existed along the front in this region. A cloud cluster developed south of the front around (31°N, 118°E) in mountain areas (see Fig. 1) favoring the formation of convective systems during the Meiyu/Baiu season (e.g., Ding 1992). Some cold IR clouds were also observed north of the front around (110–120°E). By 0800 LST, a rainband developed

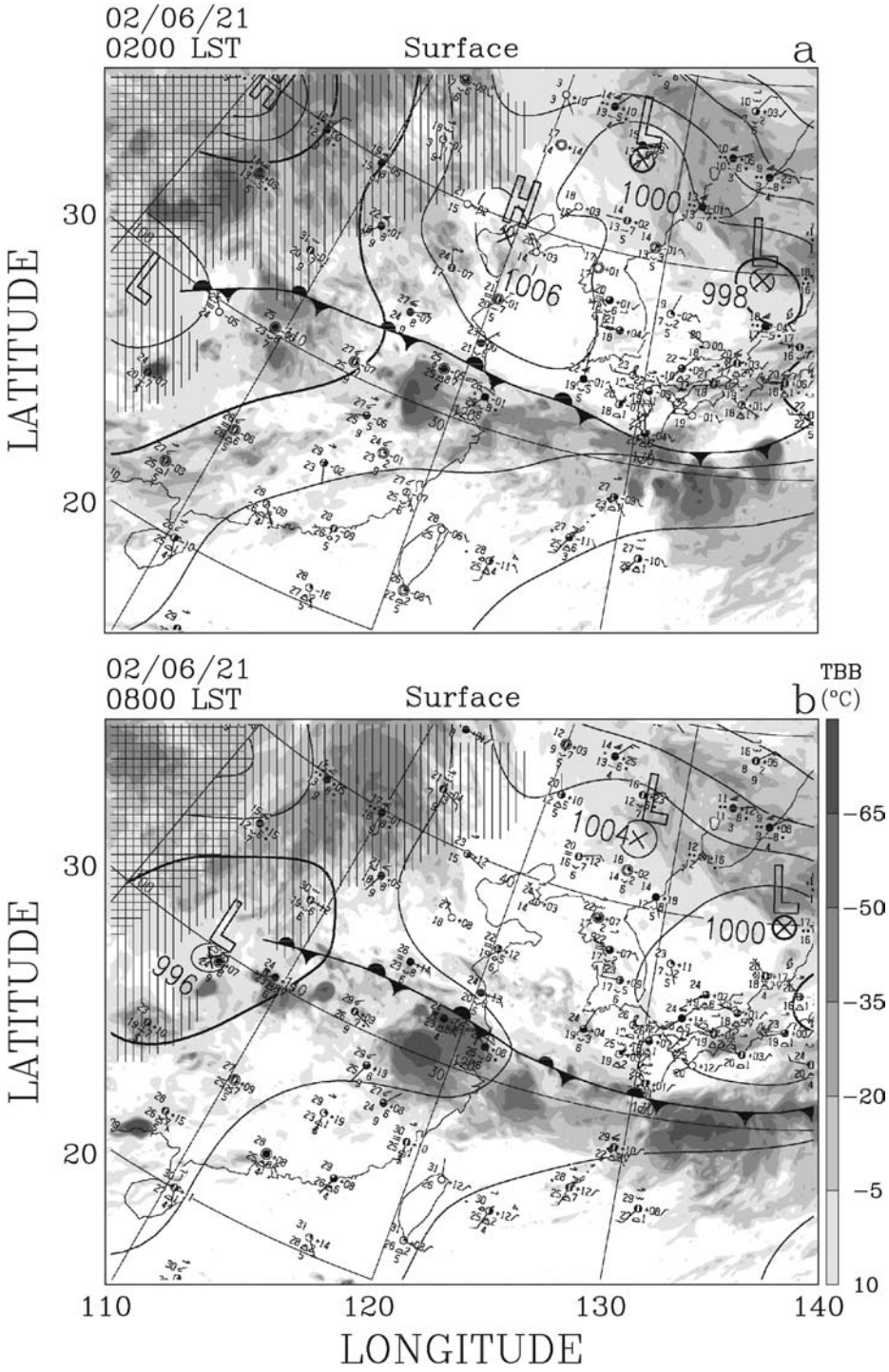

Fig. 2. Surface weather maps superimposed with GMS infrared imageries for (a) 0200 LST, and (b) 0800 LST 21 June 2002. Vertically and crosswise hatched regions represent the areas where topographic altitudes are between 1000 m between 3000 m and higher than 3000 m, respectively.

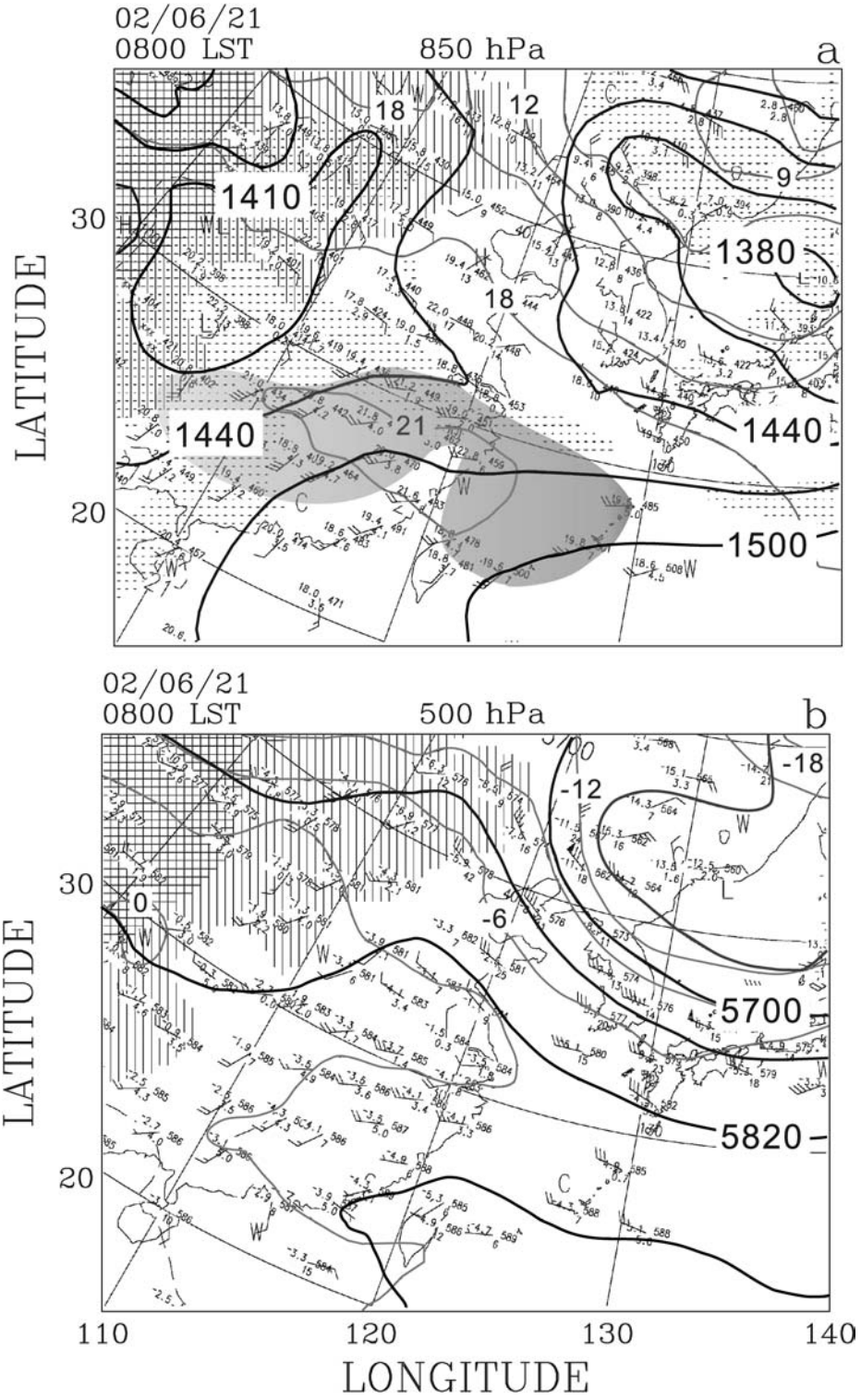

Fig. 3. Synoptic weather maps for 0800 LST 21 June 2002 at (a) 850 hPa, and (b) 500 hPa. Black lines represent geopotential heights (contoured every 50 m) and grey lines represent temperatures (contoured every 3°C). Vertical and cross hatches have the same meanings as those in Fig. 2. Dotted regions indicate the areas where the difference between temperature and dew point temperature is less than 3°C. The shaded region in (a) outlines the area with wind speeds greater than 12 m s^{-1}.

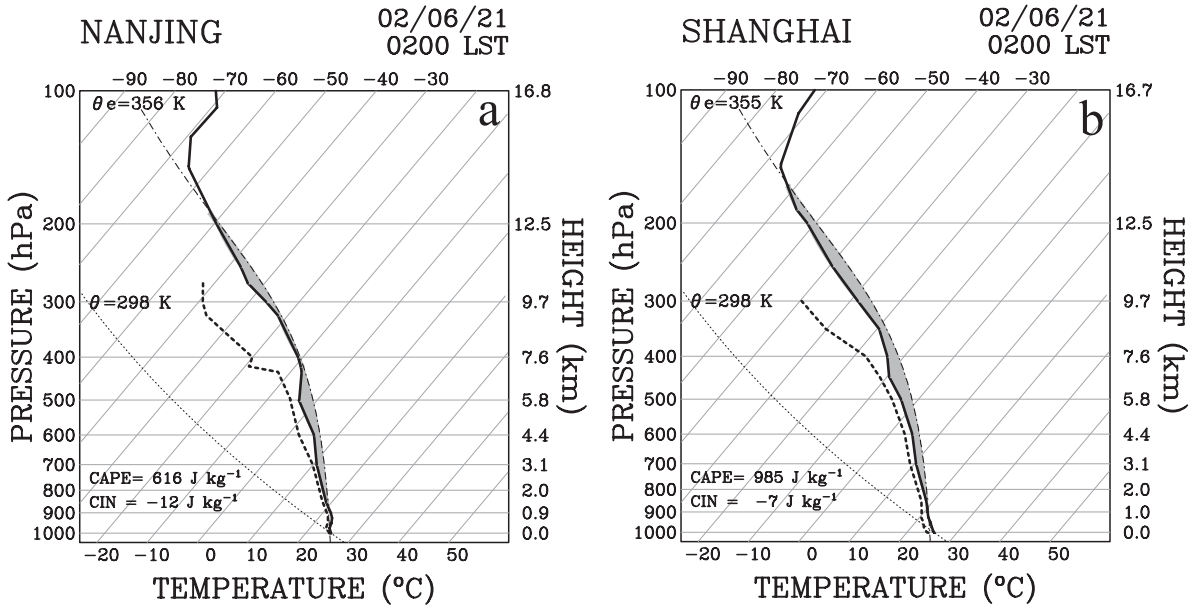

Fig. 4. Skew-T log p diagrams of temperature (bold solid line) and dew point temperature (bold dashed line) at 0200 LST 21 June 2002 from soundings at (a) Nanjing and (b) Shanghai. The shaded region in each figure indicates the positive area (CAPE).

along the front over the downstream region of the Yangtze River (Fig. 2b). The rainband was a meso-α-scale convective system (Orlanski 1975). Note that the rainband was featured by the TBB (equivalent blackbody temperature) as low as -65°C in the western part.

Ambient atmospheric stratifications (i.e. vertical structures of atmospheric temperature and humidity) ahead of the front before the formation and development of the rainband along the front are shown in Fig. 4 by using data from upper-air soundings for 0200 LST at Nanjing (NJ) and Shanghai (SH). As shown in Fig. 1, the sounding at NJ could reveal atmospheric stratifications in the western part, while the sounding at SH could reveal those in the eastern part of the downstream region of the Yangtze River.

The NJ sounding indicates that the western part was characterized by a deep layer of moisture extending from the surface to about 450 hPa (Fig. 4a). The height of the level of free convection (LFC) for a lifting air parcel from the surface was at 873 hPa (~ 1.2 km). The convective available potential energy (CAPE) and convective inhibition (CIN) were 616 J kg^{-1} and -12 J kg^{-1}, respectively. In the eastern part, the SH sounding showed similar profiles of temperature and dew point temperature as those in the western part (Fig. 4b). There also existed a deeper moisture layer from the surface. On the other hand, a lower LFC (~ 0.7 km), larger CAPE (~ 985 J kg^{-1}), and smaller CIN (~ -7 J kg^{-1}) were observed in the eastern part. It is of interest to note that the ambient atmospheric stratifications analyzed above imply that convection would have a more chance to develop intensively in the eastern part. Nevertheless, as will be analyzed in the following sections of the paper, both the front and convection were stronger in the western part than those in the eastern part of the downstream region of the Yangtze River.

In both the western and eastern parts, it is noted that the shape of the positive area (or CAPE) was tall and skinny. According to Lucas et al. (1994), such a thermal structure of the environment would be more favorable for the formation of convection with relatively deep, but weak updrafts.

4. Structure and evolution of the surface front

The structure and evolution of surface winds, divergence, and relative vorticity around the front are shown in Fig. 5. The frontal position has been de-

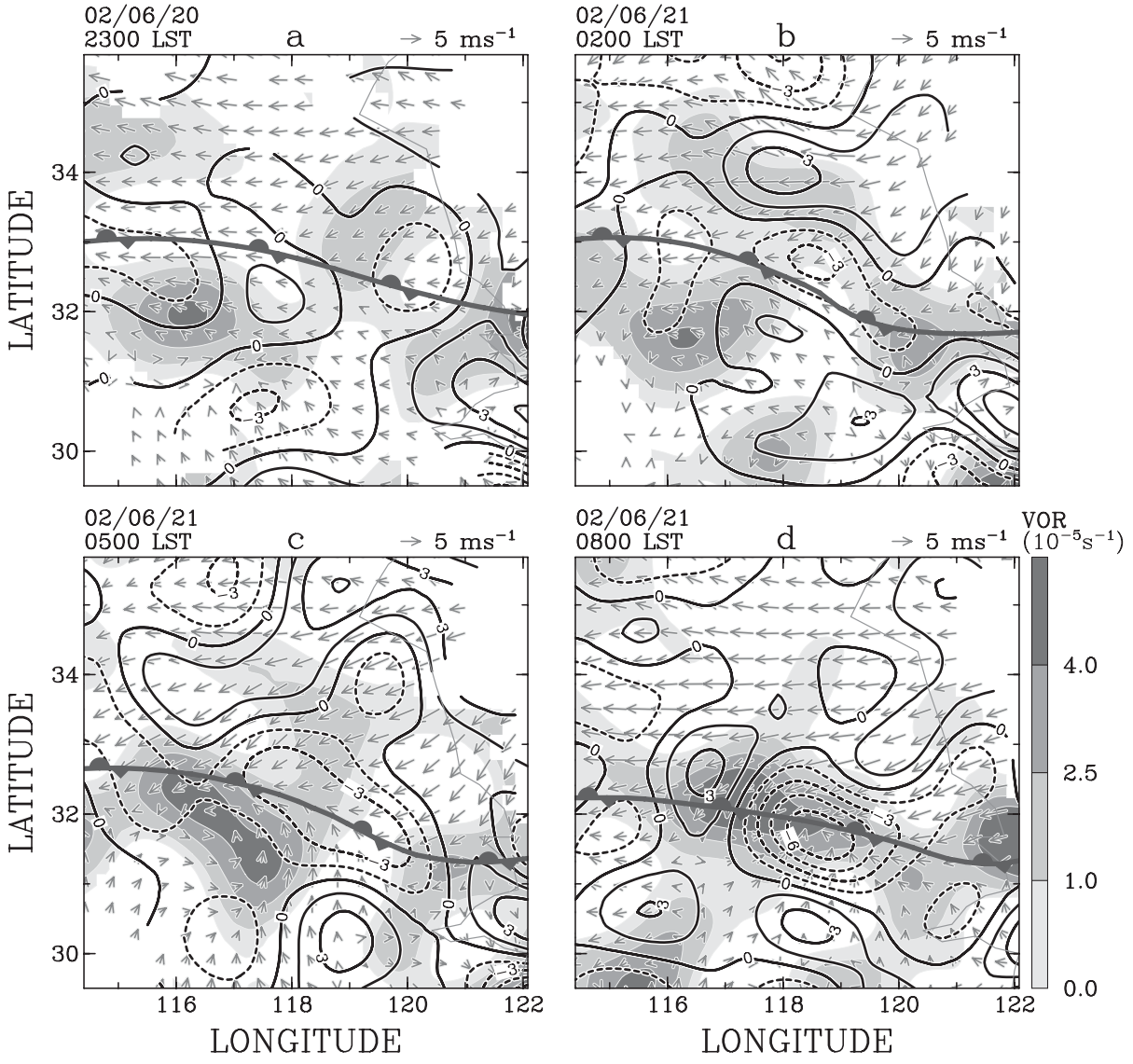

Fig. 5. Distributions of the vertical component of relative vorticity (shaded), horizontal divergence (contoured every 1.5×10^{-5} s^{-1}), and horizontal winds (arrows) at the surface for (a) 2300 LST 20 June, (b) 0200 LST, (c) 0500 LST, and (d) 0800 LST 21 June 2002. The location of the front at each time is superimposed.

termined mainly based on the strong gradient of equivalent potential temperatures (see Fig. 6) with supplementary information from winds. At 2300 LST 20 June, the front was located within a wind shift line, with east-northeasterly winds and mostly southeasterly winds immediately to the north and south, respectively (Fig. 5a). As mentioned earlier, the front was inactive before 0200 LST 21 June. In fact, the front was characterized by weak positive or negative vorticity till this time (Figs. 5a–b). The front and wind shift line were moving slowly southward after 0200 LST. From 0500 LST, positive vorticity began to increase near the front (Figs. 5c–d), indicating the intensification of the front from about this time. It is noted that accompanying the intensification of the front, the rainband developed along the front as shown in Fig. 2b. By 0800 LST, a belt of positive vorticity devel-

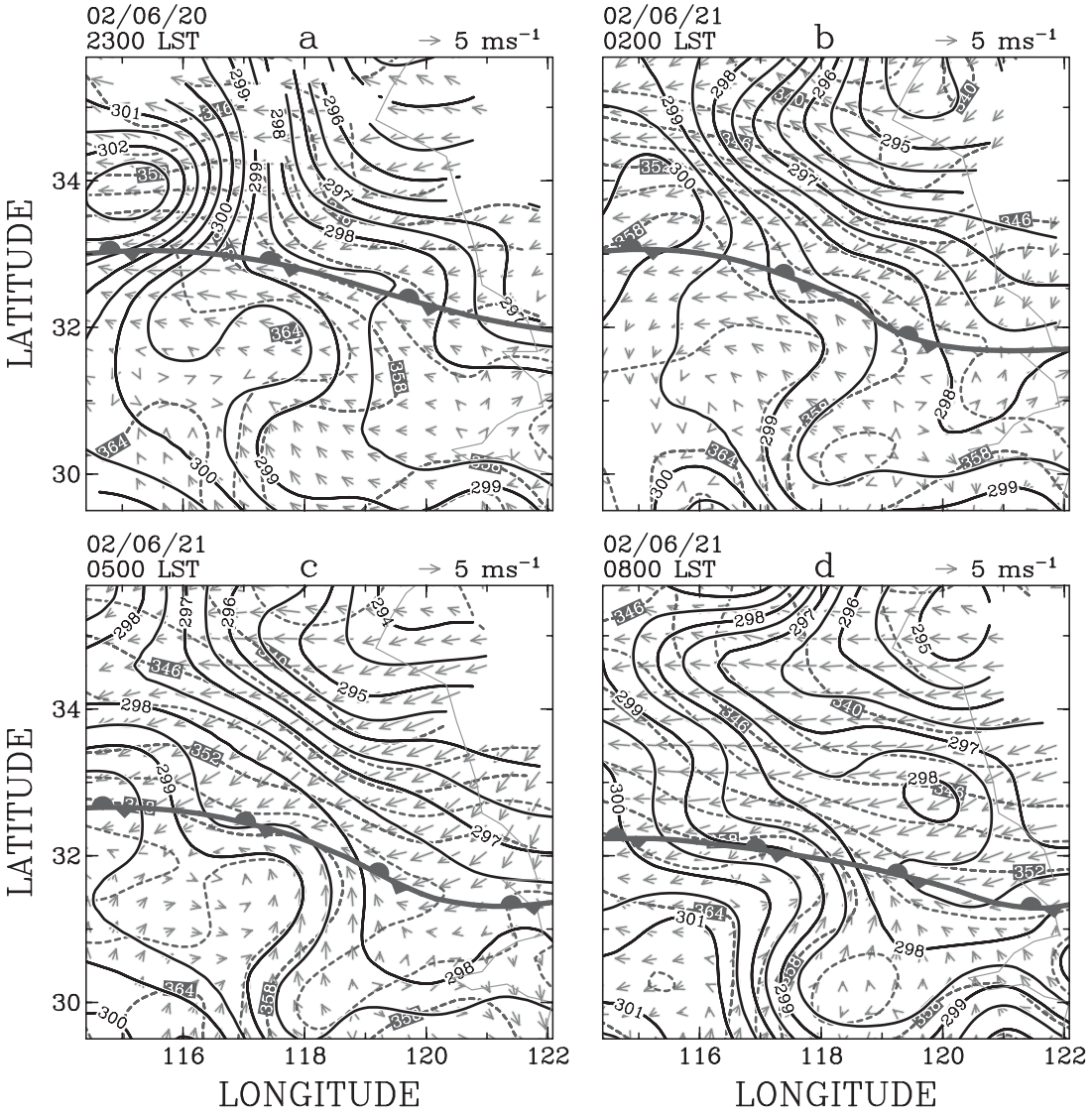

Fig. 6. Same as Fig. 5, except for potential temperature (contoured every 0.5 K by solid lines) and equivalent potential temperature (contoured every 3 K by dashed lines) at the surface.

oped along the front, with a maximum larger than 4×10^{-5} s^{-1} being located around (32.5°N, 117.0°E) (Fig. 5d).

The divergence field observed at the surface indicates that convergence along the front was weak ($\sim -1.5 \times 10^{-5}$ s^{-1}) at 2300 LST 20 June (Fig. 5a). By 0200 LST 21 June, convergence began to intensify along the front, with the most significant intensification of convergence in areas just north of the front (Fig. 5b). It is noted that the timing when convergence began to increase ($\sim$ 0200 LST) was earlier than the timing when the positive vorticity along the front started intensifying ($\sim$ 0500 LST). By 0800 LST, a strong core of convergence formed along the front (outlined by the 6×10^{-5} s^{-1} isopleth in Fig. 5d).

While the development of convergence along the front from 0200 LST was associated with both divergent southeasterly flow south of the front and divergent northeasterly flow north of the front, it is evident from Fig. 5 that stronger convergence existed north of the front and was accompanied by the intensification of northeasterly winds in a broad area. Especially, a convergence core

($\sim -3 \times 10^{-5}$ s^{-1}) formed just ahead (south) of the strongest northeasterly flow (Fig. 5b). On the other hand, it is noted that a divergence core developed further to the north around 34°N (Figs. 5b–c). Accompanying the development of the divergence core, northeasterly and east-southeasterly winds intensified simultaneously to the south and north of the divergence core, respectively.

During the intensification of northeasterly winds north of the front, a wide area of cold air was moving toward the front from the north (Fig. 6). As a result, thermal contrast across the front intensified, though the intensified thermal contrast was weaker as compared to polar fronts. By 0800 LST, it is noted that the front in the western part of the downstream region of the Yangtze River was associated with stronger vertical vorticity and horizontal convergence (Fig. 5d), higher thermal contrast (Fig. 6d) and colder IR temperature (Fig. 2b). Needless to say, both the front and associated convection underwent a stronger development in the western part than those in the eastern part of the downstream region of the Yangtze River.

5. Upper-air structure and evolution around the frontal zone

In this section, upper-air sounding data, which have been objectively processed into three dimensional grids, were used to analyze the upper-air structure and evolution around the frontal zone.

5.1 Horizontal structure and evolution

Distributions of upper-air relative vertical vorticity, horizontal divergence, and horizontal winds are shown in Fig. 7. At the 850-hPa level, the association of the front with the large-scale shear line is evident in the downstream region of the Yangtze River (Figs. 7a and 7d). At this level, strong southwesterly winds related to the LLJ were observed south of the front. From 0200 LST to 0800 LST 21 June, wind speeds on both sides of the front increased. Especially, the LLJ developed in the eastern part of the downstream region of the Yangtze River at 0800 LST. Note that both cyclonic vorticity and convergence along the front increased during this period, with maximum vorticity greater than 8×10^{-5} s^{-1} and maximum convergence of the magnitude greater than 3.0×10^{-5} s^{-1} being found in the western part. Figure 7d also indicates that the development of convergence along the front was associated with the intensification of east-northeasterly winds north of the front.

At the 500-hPa level, westerly winds prevailed immediately south and north of the front at 0200 LST (Fig. 7b). By 0800 LST, winds north of the front became more northwesterly and winds south of the front became more southwesterly. Evident is the increase in cyclonic vorticity and convergence over the front associated with the change in the wind field at the 500-hPa level. Indeed, maximum vorticity at 0800 LST became larger than 4×10^{-5} s^{-1}, which was twice as large as that observed at the previous time. Meanwhile, the magnitude of maximum convergence at 0800 LST increased to be more than 6×10^{-5} s^{-1}, which was four times larger than that observed at 0200 LST. Note that both maximum vorticity and maximum convergence at the 500-hPa level were also located in the western part.

At the 300-hPa level, winds south of the front changed from west-northwesterlies at 0200 LST to north-northwesterlies at 0800 LST (Figs. 7c and 7f). Accompanying this change, a core of convergence and a core of cyclonic vorticity developed south of the front at high levels.

5.2 Vertical structure

Previous analyses indicate that the front and convection along the front underwent a stronger development in the western part of the downstream region of the Yangtze River. Vertical cross sections at 0800 LST 21 June have been analyzed to demonstrate in detail the distinct structures of the front between the western and the eastern parts after it has developed. These vertical cross sections were normal to the rainband and also nearly normal to the front.

5.2.1 Vertical structure in the western part

Figure 8 shows the vertical structure of the frontal zone in the western part of the downstream region of the Yangtze River. In the vertical cross section showing the distribution of the cross-frontal component of winds (Fig. 8a), the interface of the positive and negative components below about 400 hPa was nearly vertical from the surface. This interface, which also represented the wind shear line, sloped northward with height at 0200 LST (not shown). It became steep with the intensification of winds north of the front at 0800 LST. Meanwhile, a region of the intense vertical shear of along-frontal winds extended over the front to about 600 hPa (Fig. 8b). Figure 8a also indicates that low-level southwesterly winds (negative components) south of the front, which was associated

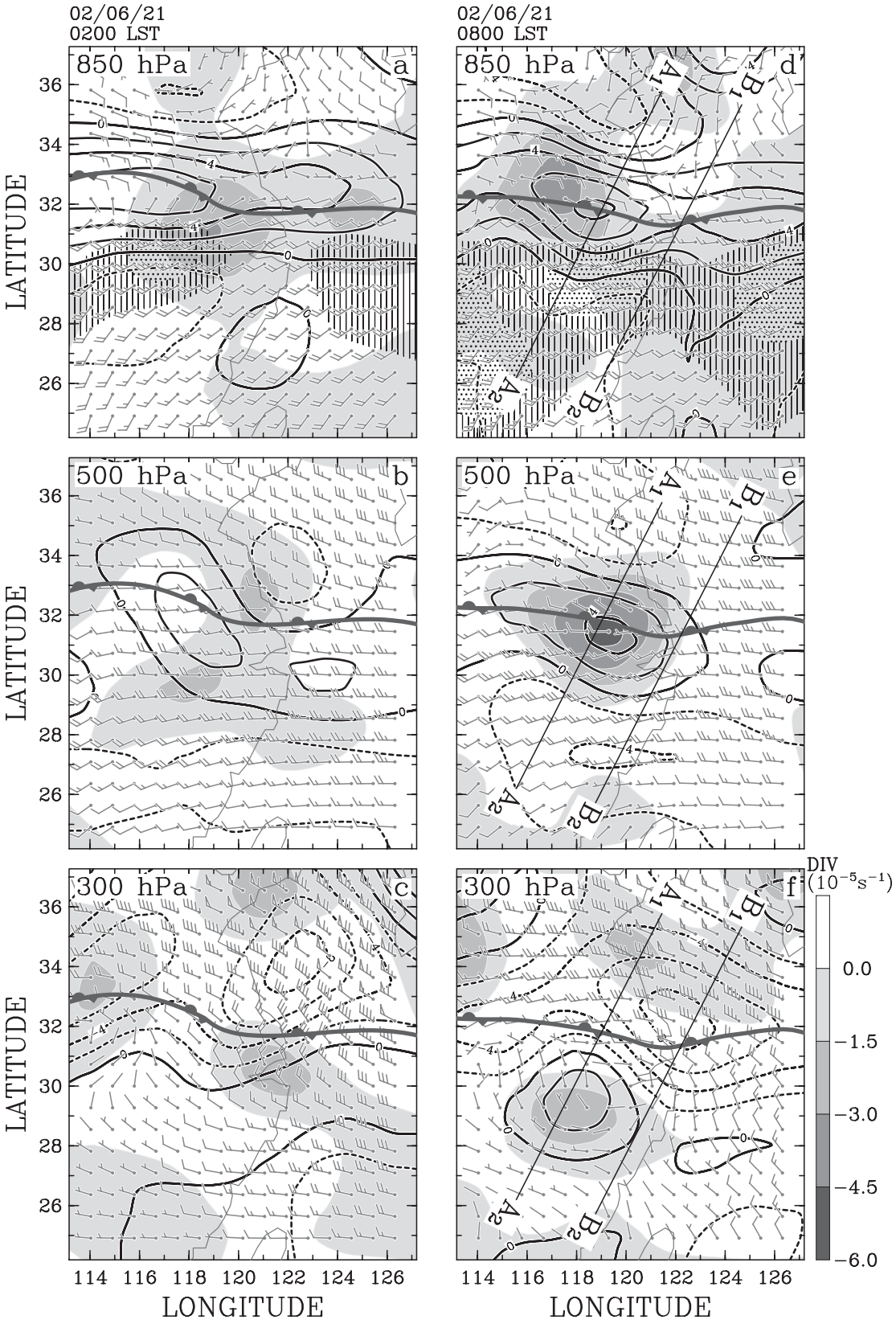
02/06/21
0200 LST
02/06/21
0800 LST
850 hPa
a
850 hPa
d
500 hPa
b
500 hPa
e
300 hPa
c
300 hPa
f
A1
B1
A2
B2
LATITUDE
LONGITUDE
36
34
32
30
28
26
114 116 118 120 122 124 126
DIV
(10⁻⁵s⁻¹)
0.0
−1.5
−3.0
−4.5
−6.0

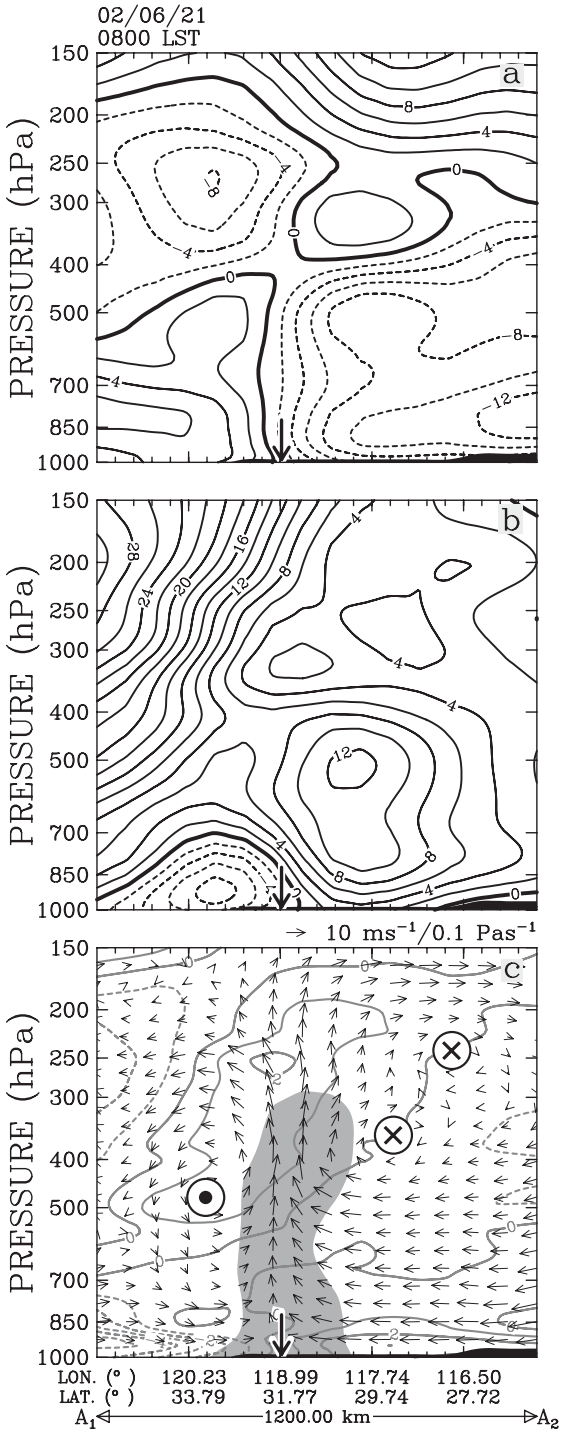

Fig. 8. Vertical cross sections for 0800 LST 21 June 2002 along line A_1A_2 in Fig. 7 for (a) the velocity of the wind component along the section plane (contoured every 2 m s^{-1}), (b) the velocity of the wind component normal to the section plane (contoured every 2 m s^{-1}), and (c) anomalies of temperature (contoured every 1 K), circulation along the vertical section plane (arrows), and relative humidity greater than 90% (shaded). The temperature anomaly was the deviation from the mean at each height. In each figure, the vertical arrow indicates the approximate position of the surface front and the topography is shaded black. The ⊙ and ⊗ in (c) indicate the centers of vertical circulations with their directions out of and into the page, respectively.

with the LLJ as seen in Fig. 7d, rose up to high levels before it went to the rear of the front. In the western part, accompanying the development of deep upward motion over the front, a region of high relative humidity (> 90%) extended up from the surface till 300 hPa (Fig. 8c). This indicates that there existed strong convection in the western part.

Two vertical circulations are evident in Fig. 8c. The vertical circulation centered at about 500 hPa behind (north of) the surface front was apparently associated with the Meiyu/Baiu front. Hereafter, this vertical circulation will be referred to as cross frontal circulation. The other vertical circulation was centered in the middle troposphere ahead (south) of the surface front. Hereafter, this vertical circulation will be referred to as prefrontal vertical circulation. The prefrontal vertical circulation could also be found at 0200 LST and was intensifying from that time (not shown). Figure 8c indicates that multiple centers existed within the prefrontal vertical circulation. It is noted that the prefrontal vertical circulation was toward the opposite direction of the cross frontal circulation. Its upward branch was associated with warmer air to the

Fig. 7. Distributions of the vertical component of relative vorticity (contoured every 2×10^{-5} s^{-1}), horizontal divergence (shaded), and horizontal winds (full barb = 5 m s^{-1} and half barb = 2.5 m s^{-1}) for 0200 LST 21 June 2002 at the (a) 850-hPa level, (b) 500-hPa level, and (c) 300-hPa level. (d)–(f) are the same as (a)–(c), except for 0800 LST 21 June 2002. Locations of the surface front are superimposed. Line A_1A_2 and line B_1B_2 indicate the locations of vertical cross sections shown in Figs. 8 and 9, respectively. Vertical hatches and dots in (a) and (d) outline areas with wind speeds between 12 m s^{-1} between 14 m s^{-1} and greater than 14 m s^{-1}, respectively.

north, while its downward branch was associated with colder air to the south. It is noted that the intensification of southerly winds at the 500-hPa level and northerly winds at the 300-hPa level south of the front (see Figs. 7e–f) was associated with the development of the prefrontal vertical circulation.

5.2.2 *Vertical structure in the eastern part*

Figure 9 shows the vertical structure of the frontal zone in the eastern part of the downstream region of the Yangtze River. There is a remarkable difference of wind structures around the front in Fig. 9 when compared with Fig. 8. The interface of the positive and negative cross-frontal wind components in the eastern part remained a considerable slope from the surface to about 600 hPa (Fig. 9a). Low-level winds north of the front in the eastern part were much weaker than those in the western part (Figs. 9a–b). On the other hand, the cross-frontal component of the LLJ overran the front from low levels. Although the lift up of prefrontal low-level air by the front is evident, the rising prefrontal air got across the front at lower levels and possessed a considerable northward inclination (Fig. 9c). Meanwhile, the shear associated with along-frontal winds was weaker than that in the western part (Fig. 9b). These facts indicate that the front in the eastern part was shallower and weaker and possessed a gentler slope than that in the western part of the downstream region of the Yangtze River. Upward motion over the front in the eastern part was also much weaker than that in the western part (Fig. 9c). Corresponding to the weaker upward motion, a region of high relative humidity ($> 90\%$) only extended up to 600 hPa, indicating that convection in the east part was much weaker.

Two distinct vertical circulations similar to those observed in the western part were also observed in the eastern part (Fig. 9c). Nevertheless, the cross frontal circulation in the eastern part was much weaker than that in the western part. Its center was located at about 850 hPa, much lower than that in the western part. On the other hand, the prefrontal vertical circulation was more consolidated than that in the western part.

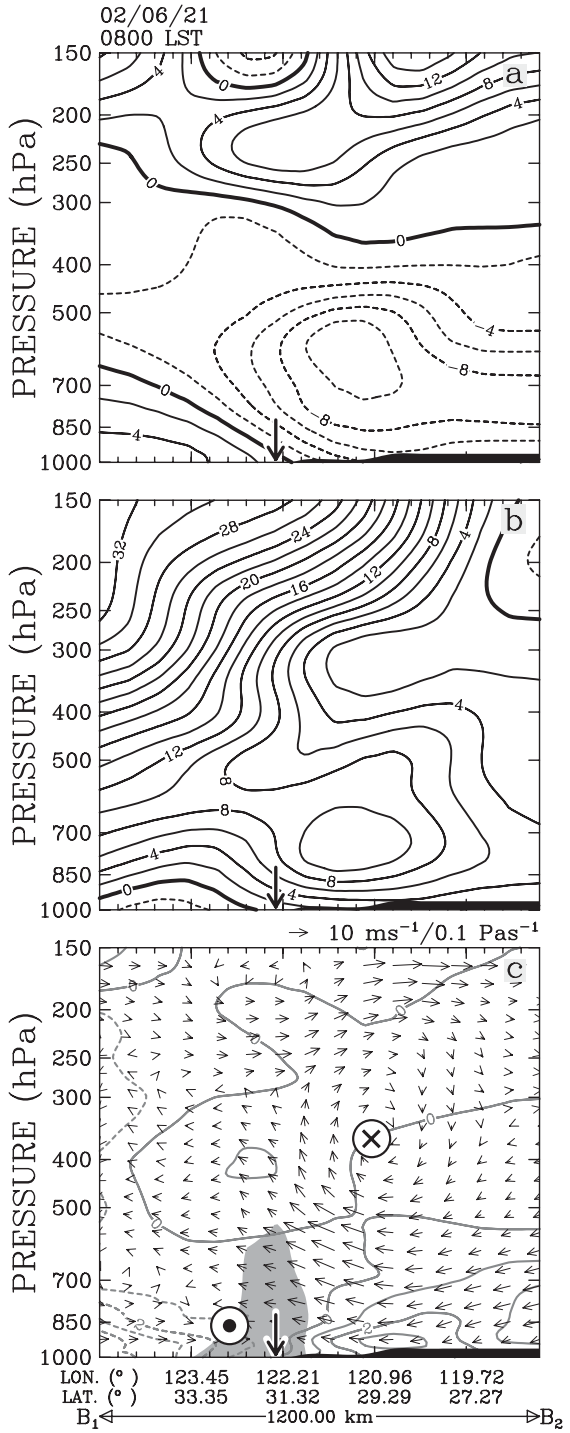

Fig. 9. Same as Fig. 8 except for vertical cross sections along line B_1B_2 in Fig. 7.

6. Fine structure and evolution of the front and precipitation

In this section, data from five Doppler radars were used to analyze the fine structure and evolution of the front and precipitation developed along

the front in the downstream region of the Yangtze River.

6.1 *Overview of the precipitation*

The perspective of precipitation systems developed around the front as revealed by the HF radar is shown in Fig. 10. It is evident that little rain existed along the front at 0200 LST 21 June (Fig. 10a). At this time, topographic-enhanced precipitation developed south of the front. The meso-α-scale convective rainband as long as 400 km formed and developed along the front from about 0400 LST (Figs. 10b–f). Several meso-β-scale convective systems (Orlanski 1975) evolved within the rainband.

The structure and evolution of meso-β-scale convective systems in the western part were distinct from those in the eastern part, especially after 0500 LST. In the western part, meso-β-scale convective systems evolved into narrow and consolidated convective lines. These convective lines propagated southward and lasted for a longer time. On the other hand, meso-β-scale convective systems in the eastern part were loosely organized and weakly developed linear convective systems. Evident is the northward extension of radar echoes in the eastern part. Apparently, meso-β-scale convective systems within the rainband have developed more strongly in the western part than those in the eastern part.

6.2 *Evolution of the front and a meso-β-scale convective system in the western part*

Figure 10 indicates that a linear meso-β-scale convective system formed and developed along the front within the western domain for the Doppler radar analysis after 0500 LST 21 June. Shown in Fig. 11 are horizontal sections of radar reflectivity and horizontal winds of the meso-β-scale convective system observed in the western domain at 0536 LST. At the 1.0-km level, strong linear radar echoes were located just north of a wind shear line related to the front (Fig. 11a). Southwesterly winds and easterly winds generally existed to the south and north of the front, respectively. The wind shear line could also be recognized at the 3.0-km level (Fig. 11b). On the other hand, southwesterly winds predominated at the 6.5-km level (Fig. 11c). At this level and the 10.0-km level (Fig. 11d), it is noted that northwesterly winds were observed. It appears that wind structures revealed by Doppler radars were generally similar to those analyzed from the surface and upper-air observations (see Figs. 5–7).

A vertical section cut through strong radar echoes along the linear convective system at 0536 LST is shown in Fig. 12. The vertical section is also nearly parallel to the front. It is found that convective updrafts and echoes developed along the front. Figure 13 shows a vertical section across the front for 0536 LST. Evident is a strong convective cell behind the front (Fig. 13a). The intensity of the cell was greater than 40 dBZ and the top of the cell exceeded an altitude of 15 km. The magnitude of the updraft related to the cell reached about 4.5 m s^{-1}. It appears that the structure of the cell revealed by the Doppler radar analysis was consistent with the sounding observation that indicated the formation of taller convection with weaker updrafts (see Fig. 4). The updraft varied with height with a maximum in the middle troposphere. The structure and magnitude of the updraft observed in this study closely resembled those of the 90th percentile of the updraft velocity in simulated GATE convection (Xu and Randall 2001). A rapid decrease of radar reflectivity with height above an altitude of 5 km (that is the height near 0°C) is also evident in Fig. 13a. As pointed out by Zipser and LeMone (1980), such a reflectivity structure was consistent with weaker updrafts retrieved from Doppler radars.

Figure 13 indicates that Doppler radars also captured the cross frontal circulation as analyzed from the upper-air observation (Fig. 8). At 0536 LST, however, the frontal surface was lower and below an altitude of 1.5 km. Over the frontal surface from altitudes of 2 km to 5 km, it is noted that an area of northerly winds (toward the right in the figure) evolved just north of the strong convective cell. The lifting of the low-level flow by the front is clearly apparent from Fig. 13b. Similar to the result of the upper-air observation (see Fig. 8), the low-level flow south of the front was lifted to higher levels before it flowed to the rear stratiform region. Note that the low-level cross-frontal flow south of the front was not so strong, with its maximum magnitude being about 6 m s^{-1} (Fig. 13b).

South of the primary updraft, stronger southerly winds (toward the left in the figure) were found around an altitude of 6 km and northerly winds existed over those stronger southerly winds. This flow structure reflected the characteristic of the prefrontal vertical circulation captured by the upper-air observation (see Fig. 8). It is noted that the primary updraft shown in Fig. 13a sloped northward largely (toward the left in the figure) at low levels and became nearly upright above an altitude of 6 km. Although the reason why the primary up-

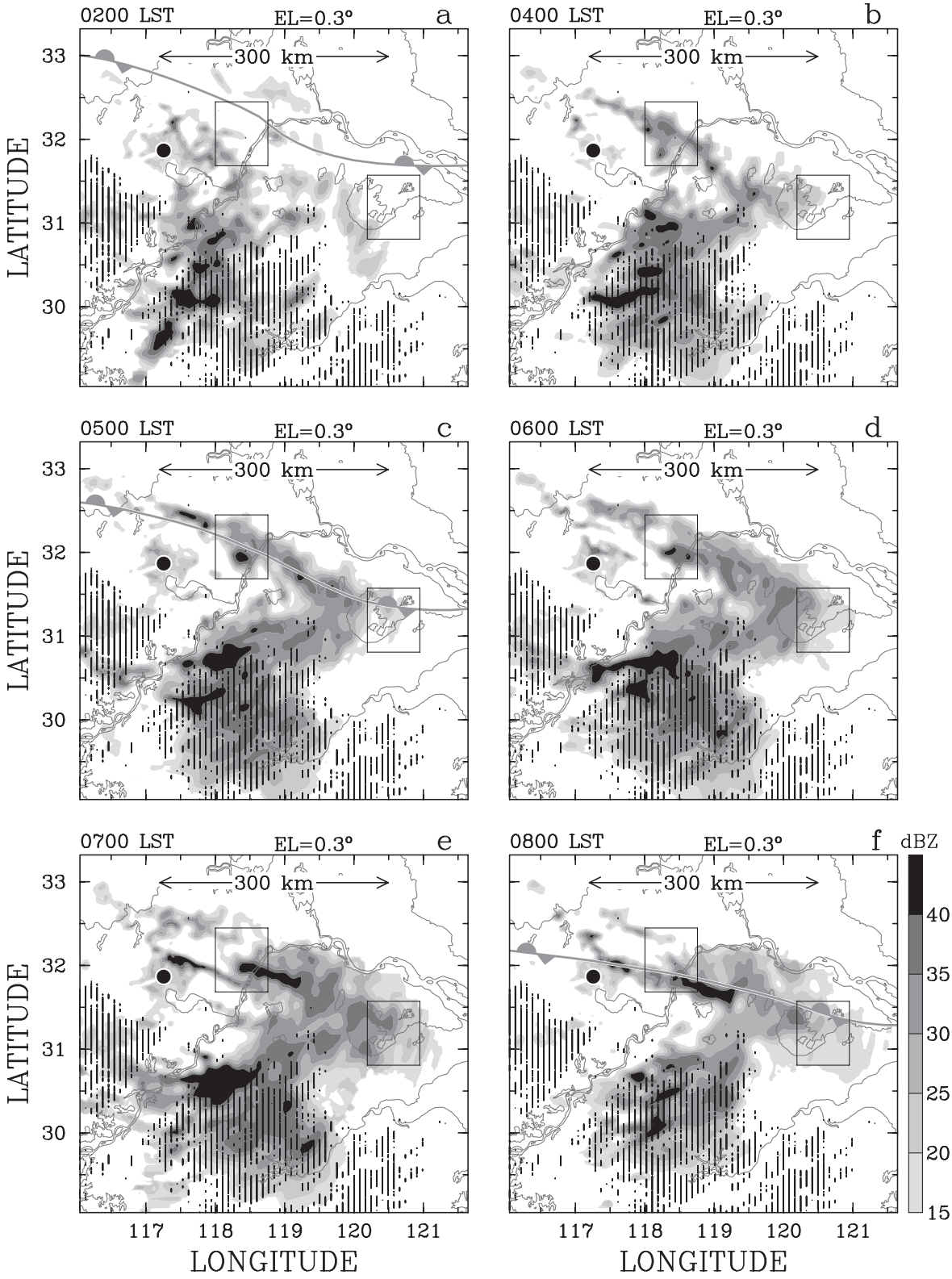

Fig. 10. Reflectivity patterns obtained from low-elevation PPI scans of the HF radar for (a) 0200 LST, (b) 0400 LST, (c) 0500 LST, (d) 0600 LST, (e) 0700 LST, and (f) 0800 LST 21 June 2002. The • indicates the location of the HF radar. Locations of the Meiyu/Baiu front at 0200 LST, 0500 LST, and 0800 LST are also shown. Boxes indicate Doppler-radar analysis domains. Vertical hatches outline regions with topographic altitudes greater than 200 m.

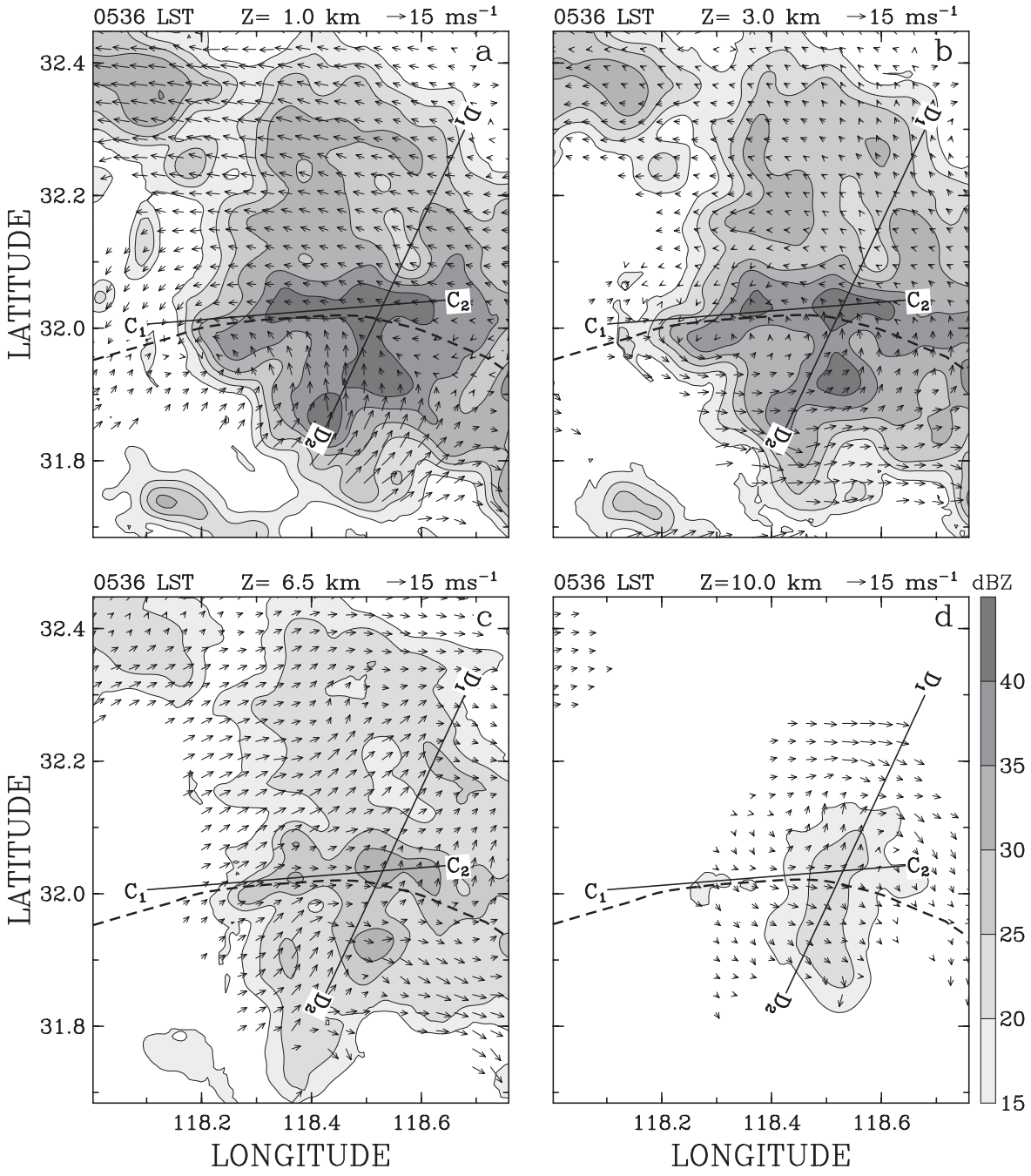

Fig. 11. Horizontal sections of radar reflectivity (shaded) and horizontal winds (arrows) in the region labeled W in Fig. 1 for 0536 LST 21 June 2002 at the (a) 1.0-km level, (b) 3.0-km level, (c) 6.5-km level, and (d) 10.0-km level. Line C_1C_2 and line D_1D_2 indicate the locations of vertical cross sections shown in Figs. 12 and 13, respectively. The dashed line in each figure outlines the shear line associated with the front at the 1.0-km level.

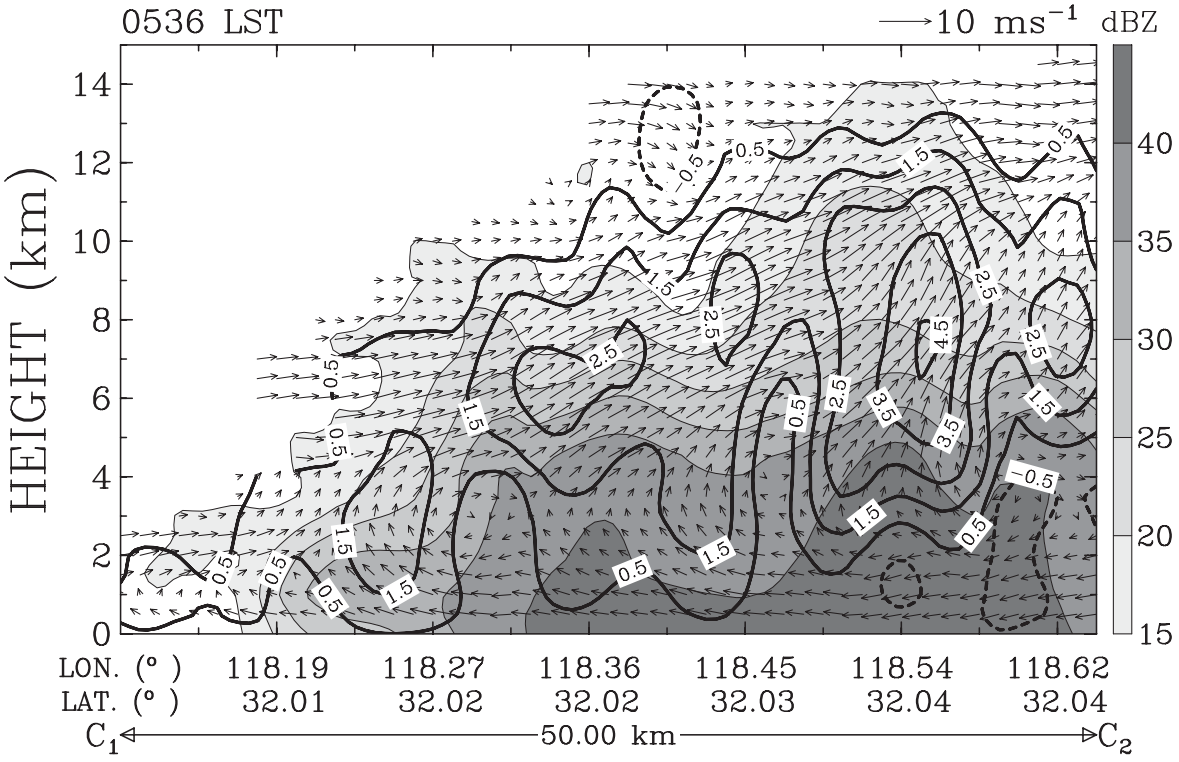

Fig. 12. Vertical cross section of radar reflectivity (shaded), winds along the section plane (arrows), and vertical velocity (contoured every 1 m s^{-1}) for 0536 LST 21 June 2002. The section is along line C_1C_2 in Fig. 11.

draft became erect was not clear, the erect updraft provided an optimal condition for the convection to develop deeply (Rotunno 1988). On the other hand, it is found that convective echoes south of the front were shallow and have never developed deeply.

During the next one hour, the meso-β-scale convective system moved slightly southward (Fig. 14). The area of intense radar echoes has increased at both low and middle levels. Linear convective echoes to the south of the target convective system were associated with another meso-β-scale convective system, which is more clearly seen in Fig. 10e. It is noted that horizontal winds showed similar structures to those observed one hour before, except at low and middle levels behind the front where east-northeasterly winds became stronger in intensity.

Figures 15 and 16 depict vertical sections nearly parallel and normal to the front at 0636 LST, respectively. Convective updrafts over the front became stronger than before (Fig. 15). The frontal surface has reached a much higher height and became steeper behind the primary convective cell (Fig. 16). Meanwhile, the cross frontal circulation increased in intensity. Its center was now located at an altitude of about 6 km, similar to that indicated by the upper-air observation (see Fig. 8c). These facts suggest that the front had intensified during this period.

On the other hand, except the apparent change in the intensities of the cross frontal circulation and updrafts over the front, little change was found in the structure of the meso-β-scale convective system. Figure 16 indicates that the primary updraft and convective cell still existed just north of the front. Note that the primary updraft remained slope (upright) below (above) an altitude of 6 km. South of the primary updraft, northerly winds at high levels and strong southerly winds at middle levels could also be recognized. Meanwhile, convective echoes ahead of the front remained shallow and stratiform echoes appeared to the rear.

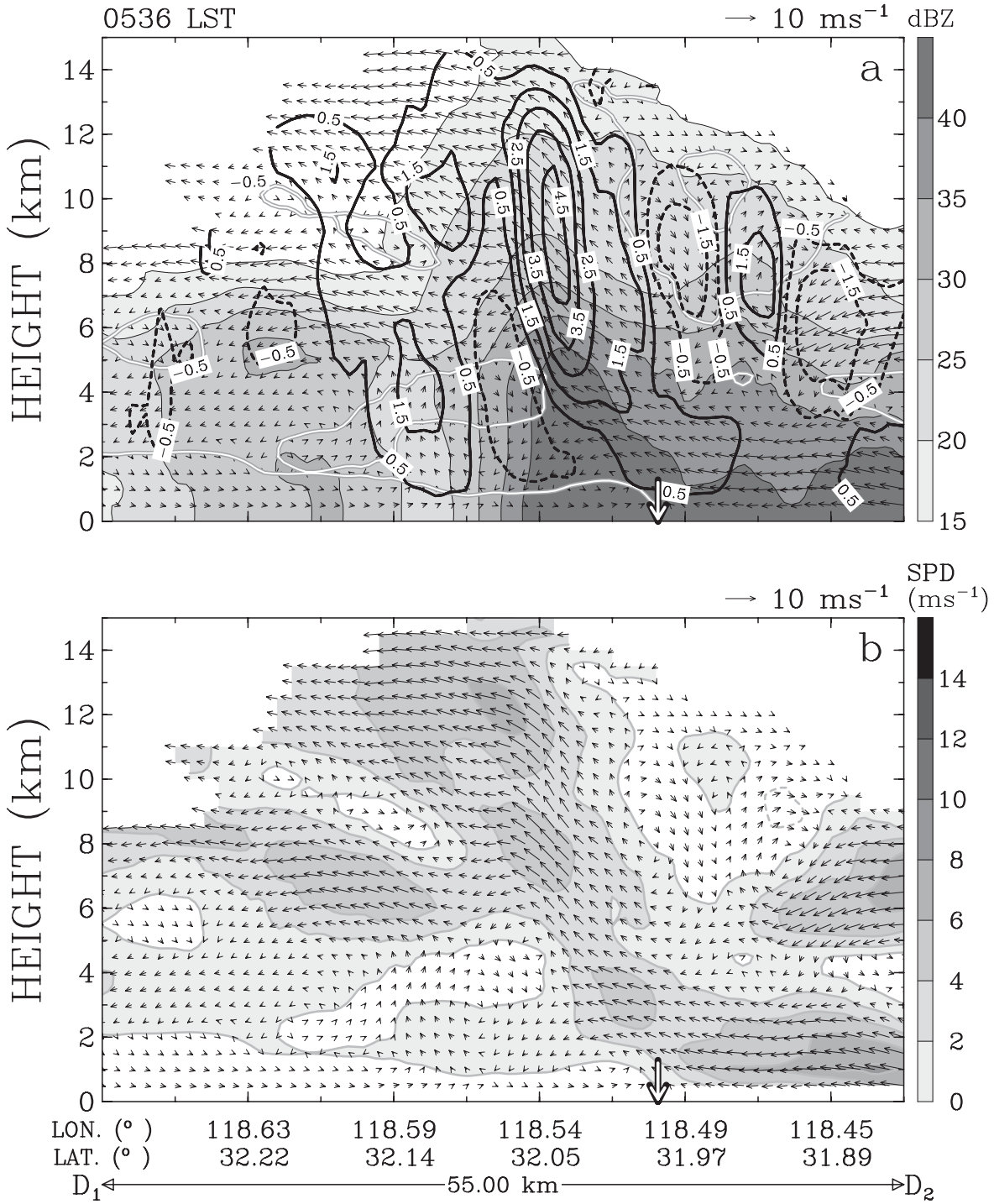

Fig. 13. (a) Vertical cross section of radar reflectivity (shaded), winds along the section plane (arrows), and vertical velocity (contoured every 1 m s^{-1}) for 0536 LST 21 June 2002. The section is along line D_1D_2 in Fig. 11. White solid lines represent interfaces of the positive and negative velocities of horizontal winds along the section plane. The approximate location of the front at the surface is indicated by the white vertical arrow. (b) Same as (a) except for the velocity of the horizontal wind component along the section plane (contoured every 2 m s^{-1} and shaded above 0 m s^{-1}).

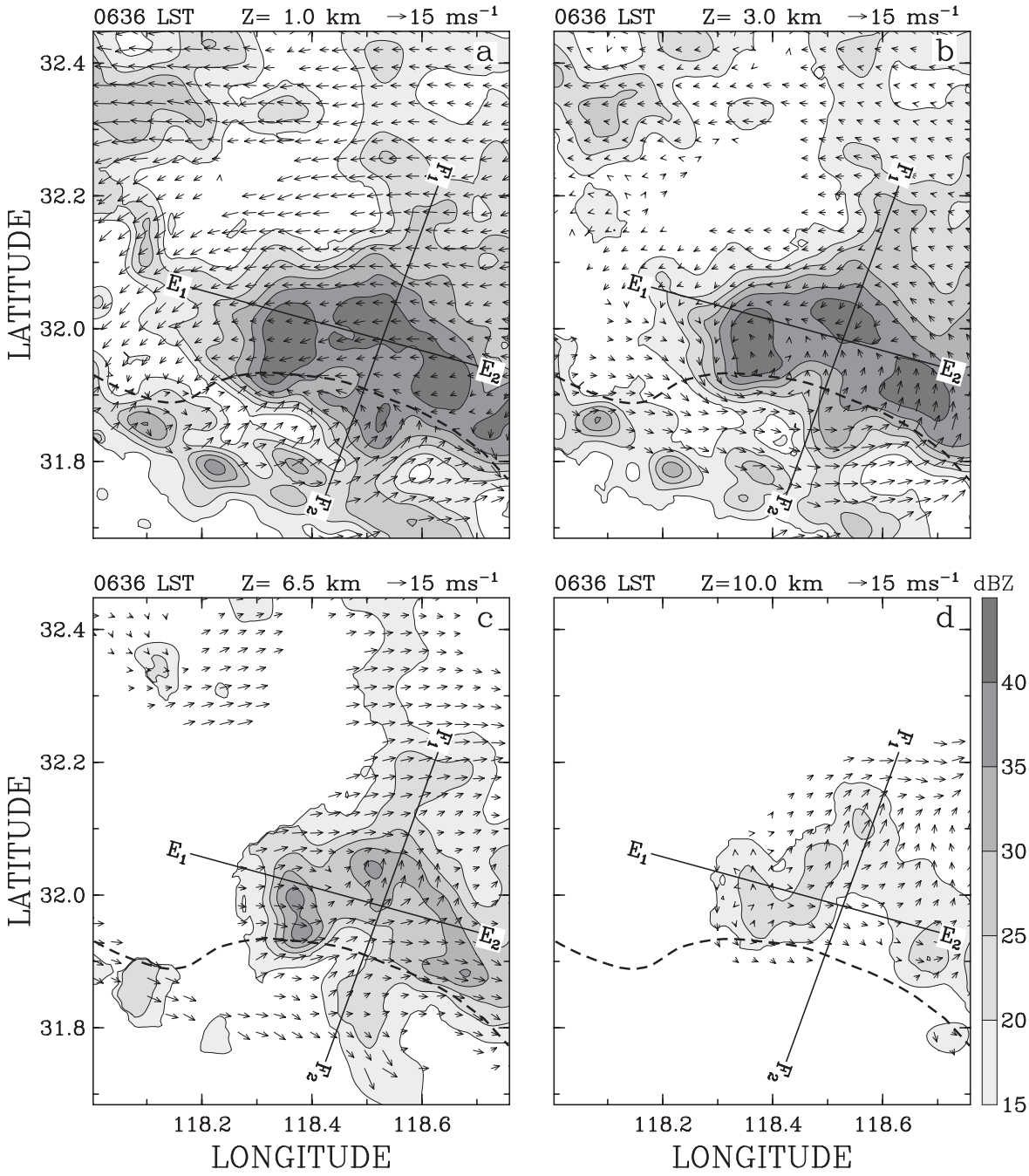

Fig. 14. Same as Fig. 11 except for 0636 LST 21 June 2002. Line E_1E_2 and line F_1F_2 indicate the locations of vertical cross sections shown in Figs. 15 and 16, respectively.

6.3 *Evolution of the front and a meso-β-scale convective system in the eastern part*

Figure 10 also indicates that another meso-β-scale convective system formed and developed along the front within the eastern domain for the Doppler radar analysis after 0500 LST 21 June. Horizontal sections of radar reflectivity and horizontal winds of the meso-β-scale convective system

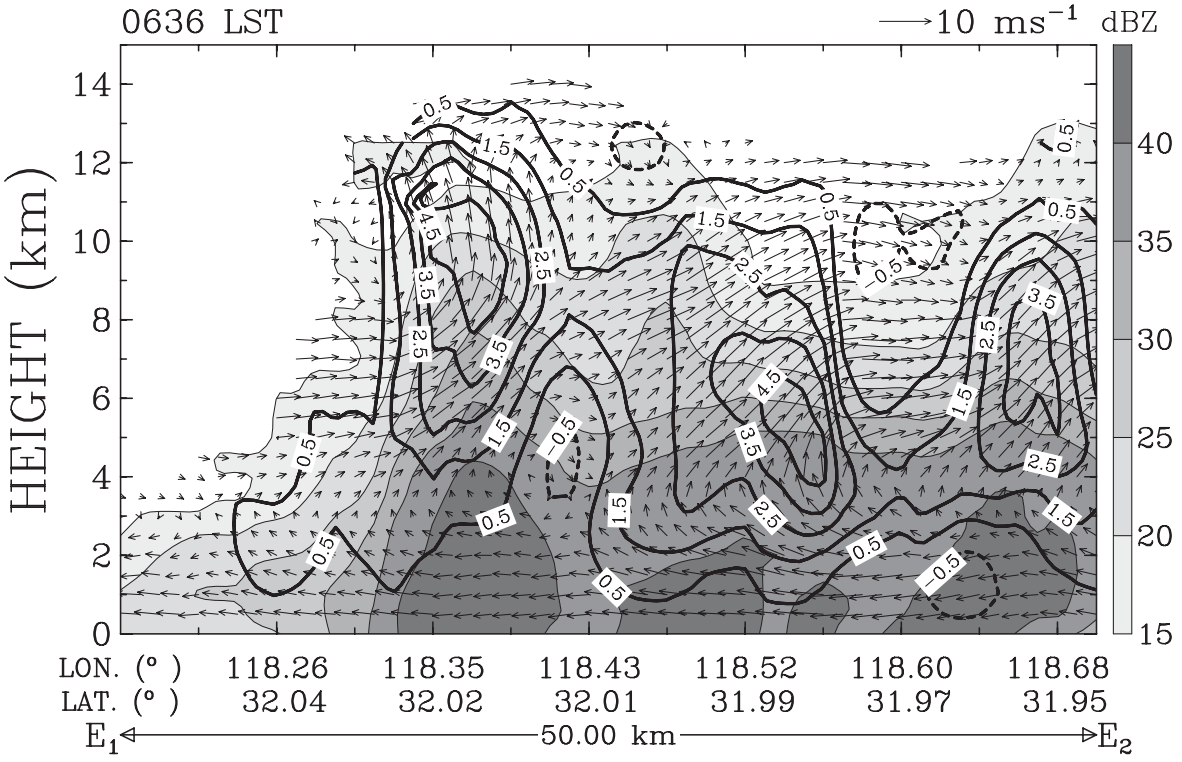

Fig. 15. Same as Fig. 12, except for 0636 LST 21 June 2002 and along line E_1E_2 in Fig. 14.

for 0648 LST in the eastern domain are shown in Fig. 17. Compared to consolidated radar echoes along the front in the western part, radar echoes in the eastern part were scattered. At the 0.5-km level, multiple linear precipitation cores appeared (Fig. 17a). Southwesterly winds appeared south of the front and northeasterly and northwesterly winds were observed north of the front. Note that winds north of the front were much weaker than those in the western part (see Fig. 11). On the other hand, much stronger southwesterly winds were found above the 0.5-km level (Figs. 17b,c). Meanwhile, west-northwesterly winds were observed at high levels (Fig. 17d).

A vertical section cut through intensive radar echoes along the linear precipitation near the front at 0648 LST is shown in Fig. 18. Like the western part (see Figs. 12, 15), convective updrafts and echoes also developed along the front in the eastern part. Nevertheless, the intensities of convective updrafts and echoes along the front in the eastern part were much weaker than those in the western part. A vertical section across the front indicates that the front in the eastern part was apparently shallow, with its height less than 1 km at 0648 LST (Fig. 19). Compared to the one primary convective updraft and cell just north of the front in the western part (see Figs. 13, 16), several updraft cores and convective cells existed across the front in the eastern part (Fig. 19a). The maximum echo top of convective cells was around an altitude of 11 km, lower than that observed in the western part. To the north of the surface front, it is noted that downdrafts dominated at low levels, even over the frontal surface. Convective echoes decreased in intensity and became stratiform echoes as they were away from the front to the north.

In the eastern part, although the front was shallow, the lifting of the low-level warm and moist flow by the front is also apparent (Fig. 19b). On the other hand, the cross-frontal flow south of the front was much stronger than that in the western part. Its speed had exceeded 12 m s^{-1} in the eastern part. Like what was observed by upper-air soundings (see Fig. 9), the low-level cross-frontal flow south of the front penetrated far to the north of

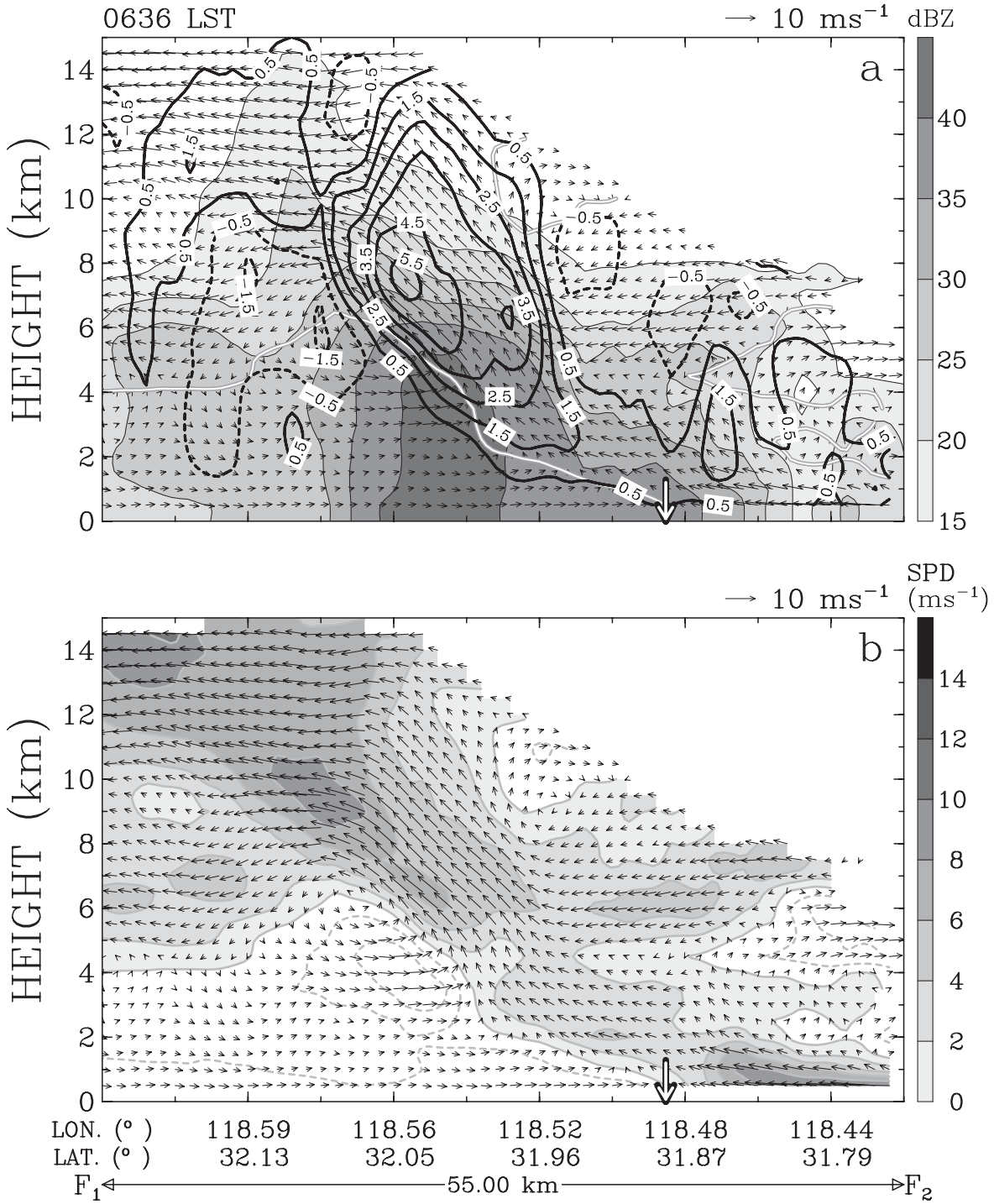

Fig. 16. Same as Fig. 13, except for 0636 LST 21 June 2002 and along line F_1F_2 in Fig. 14.

the surface front and did not go to higher levels. On the other hand, northerly winds (toward the right in the figure) existed over southerly winds. Stronger northerly winds were found just over the frontal surface at high levels. It appears that the mid- and high-level flow structure around the surface front in

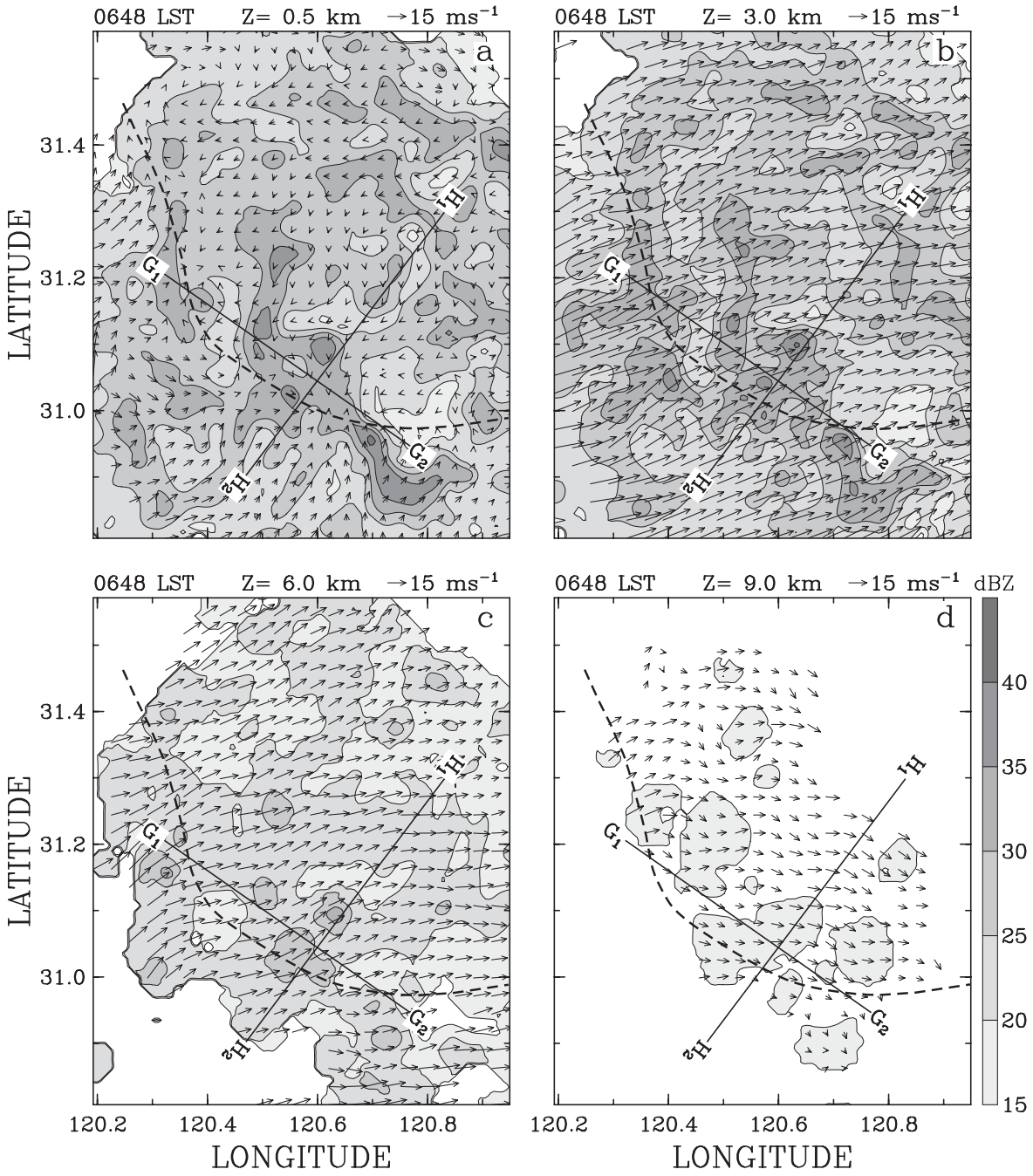

Fig. 17. Horizontal sections of radar reflectivity (shaded) and horizontal winds (arrows) in the region labeled E in Fig. 1 for 0648 LST 21 June 2002 at the (a) 0.5-km level, (b) 3.0-km level, (c) 6.0-km level, and (d) 9.0-km level. Line G_1G_2 and line H_1H_2 indicate the locations of vertical cross sections shown in Figs. 18 and 19, respectively. The dashed line in each figure outlines the shear line associated with the front at the 0.5-km level.

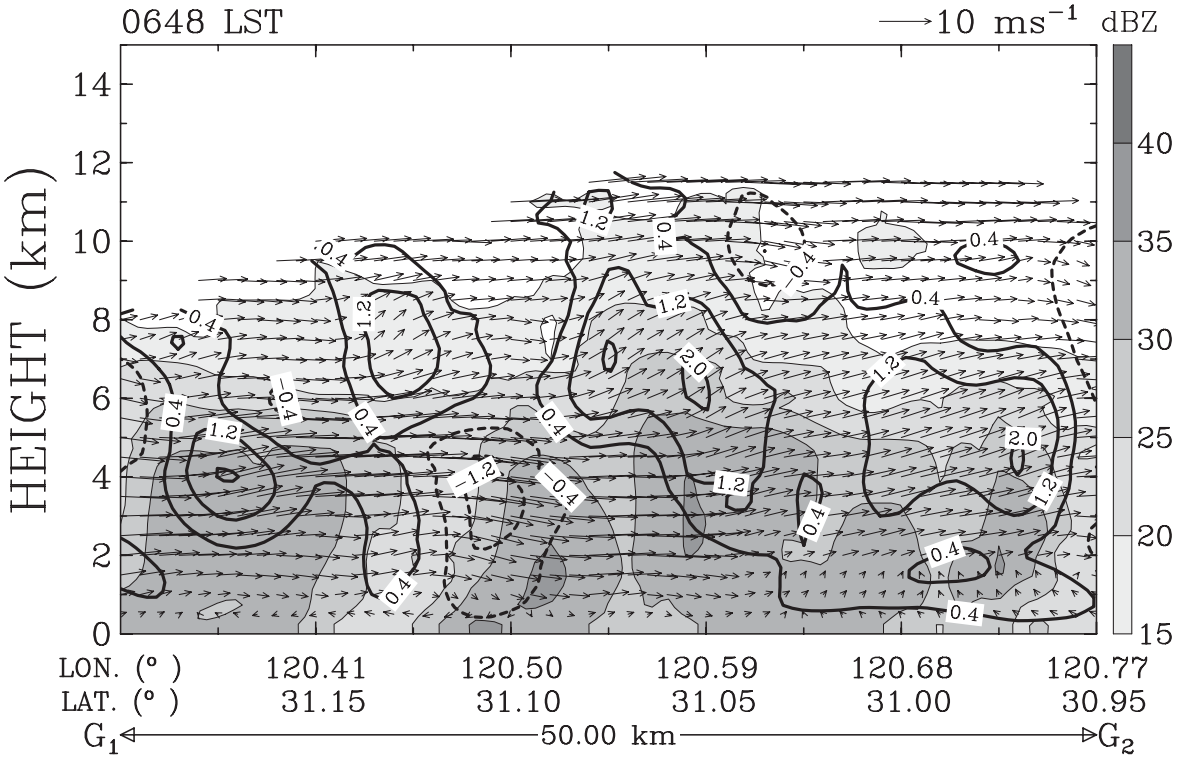

Fig. 18. Vertical cross section of radar reflectivity (shaded), winds along the section plane (arrows), and vertical velocity (contoured every 0.8 m s^{-1}) for 0648 LST 21 June 2002. The section is along line G_1G_2 in Fig. 17.

the eastern part also reflected the characteristic of the prefrontal vertical circulation observed by upper-air soundings in this region (see Fig. 9).

By 0818 LST, the front in the eastern part also intensified, which is manifested by the fact that the magnitude of winds north of the front at the 0.5-km level has increased (Fig. 20a). At this time, the front has retreated northward. Strong southwesterly winds could also be found at low and middle levels (Figs. 20b,c) and west-northwesterly winds were still observed at high levels (Fig. 20d).

In contrast to the steady structure in the western part, the structure of the convective system in the eastern part changed with time considerably. Figure 21 shows a vertical section nearly parallel to the front at 0818 LST. It is evident that downdrafts have dominated some parts along the front at this time. A vertical section across the front for 0818 LST is shown in Fig. 22. Compared to the former time (see Fig. 19), although the height of the frontal surface has increased to an altitude of 1.5 km and the intensity of updrafts has increased to 3.6 m s^{-1} (Fig. 22a), echo top heights apparently decreased, being as low as 8 km. Updrafts triggered by the front tilted northward from lower levels to echo tops. Meanwhile, a broad region of stratiform precipitation appeared south of the front.

Figure 22b indicates that the low-level flow south of the front was keeping the northward invasion over the front. On the other hand, it is noted that speeds of southerly winds at middle levels increased on both sides of the surface front at 0818 LST. At the same time, northerly winds over stronger southerly winds also intensified on both sides of the surface front.

7. Discussion

In the previous sections, the structure and evolution of a Meiyu/Baiu front and a meso-α-scale rainband developed along the front in the downstream region of the Yangtze River have been analyzed. The rainband consisted of several meso-β-scale convective systems. At the same time, the front and meso-β-scale convective systems in the western

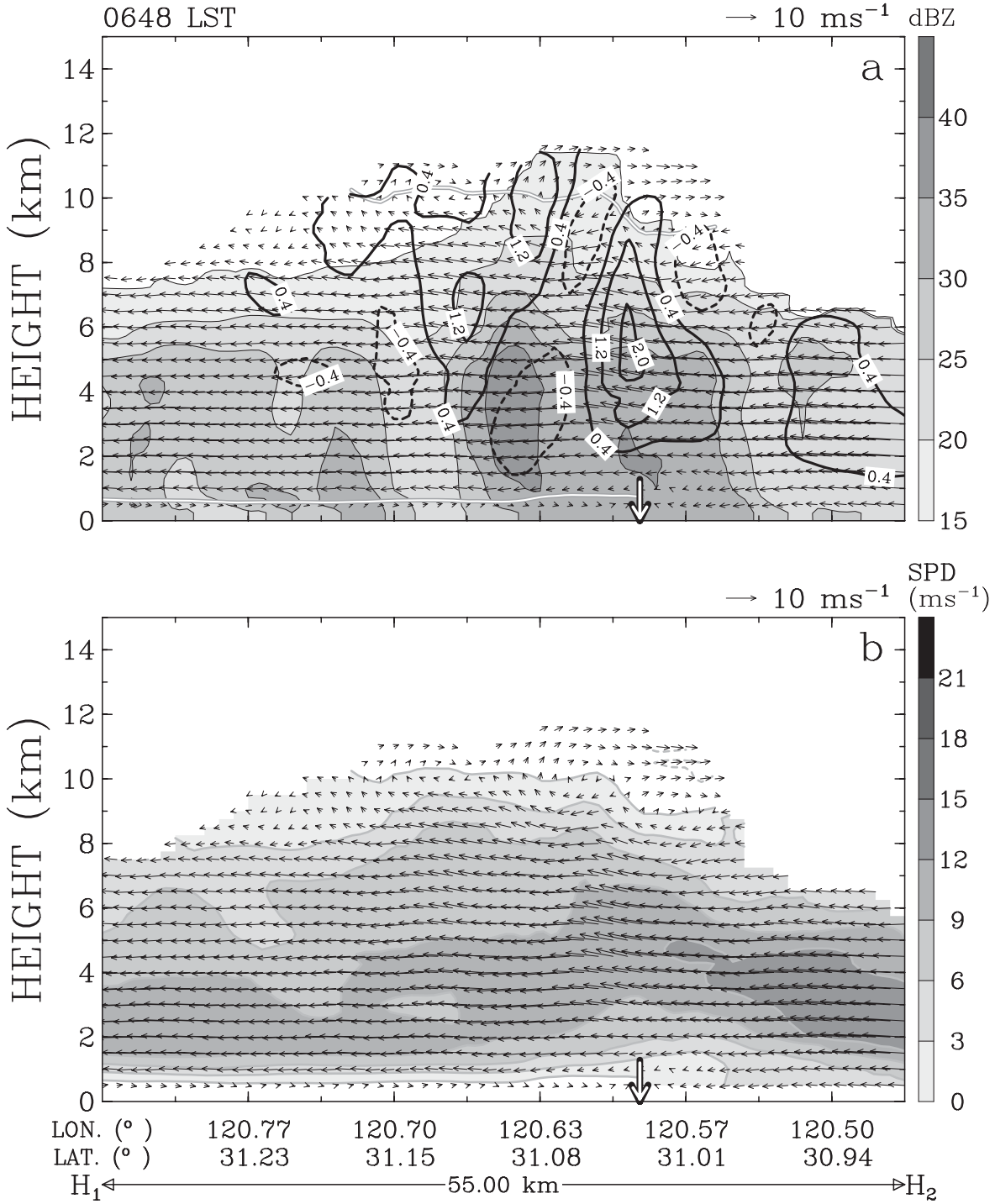

Fig. 19. (a) Vertical cross section of radar reflectivity (shaded), winds along the section plane (arrows), and vertical velocity (contoured every 0.8 m s^{-1}) for 0648 LST 21 June 2002. The section is along line H_1H_2 in Fig. 17. White solid lines represent interfaces of the positive and negative velocities of horizontal winds along the section plane. The approximate location of the front at the surface is indicated by the white vertical arrow. (b) Same as (a) except for the velocity of the horizontal wind component along the section plane (contoured every 3 m s^{-1} and shaded above 0 m s^{-1}).

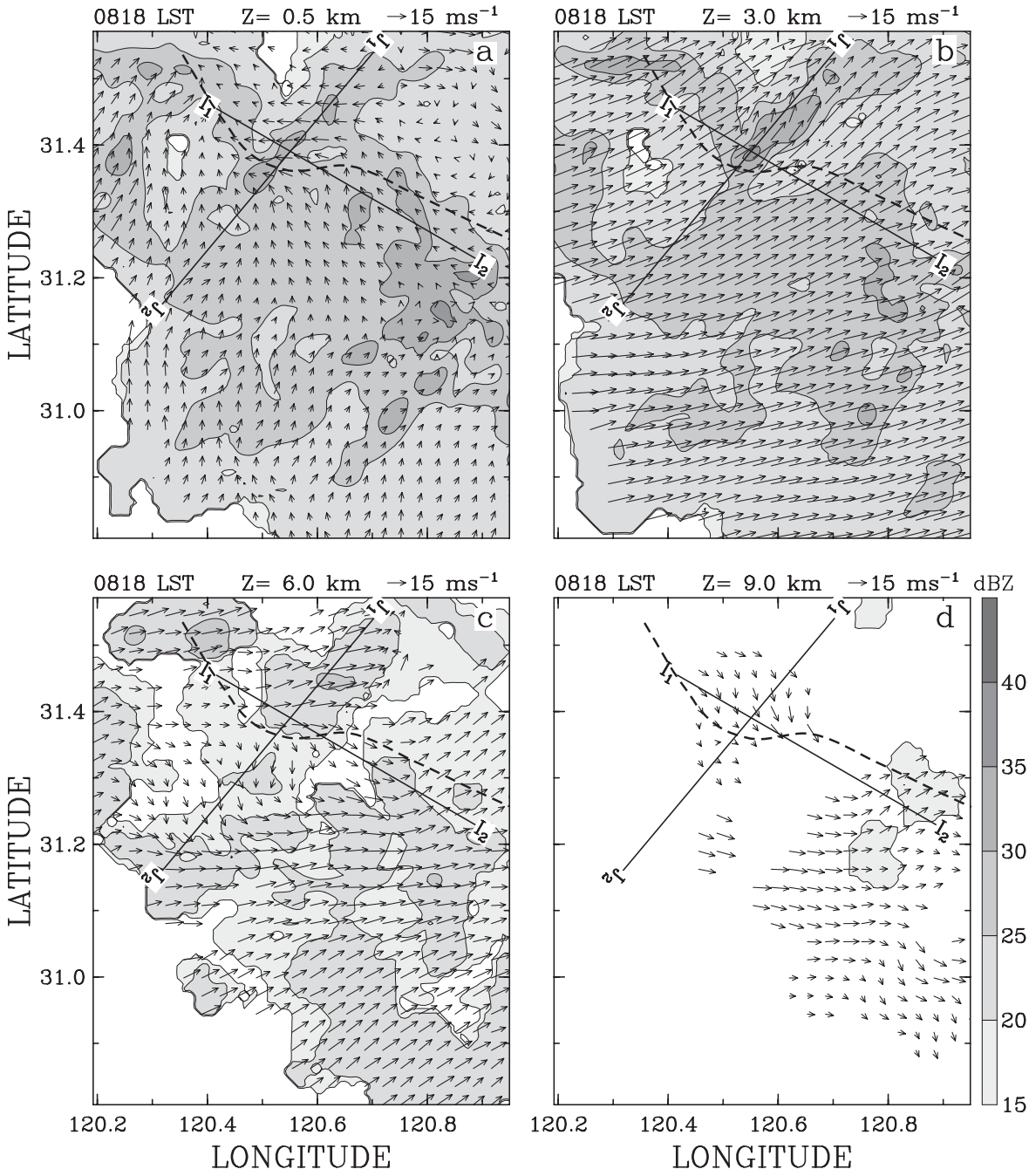

Fig. 20. Same as Fig. 17 except for 0818 LST 21 June 2002. Line I_1I_2 and line J_1J_2 indicate the locations of vertical cross sections shown in Figs. 21 and 22, respectively.

part showed the distinct structure and evolution from those in the eastern part. In this section, some important mesoscale processes related to the development and variability of the front and convective systems along the front will be discussed.

7.1 Mesoscale developing processes of the Meiyu/Baiu front

In the previous sections, it was shown that the Meiyu/Baiu front observed in the downstream region of the Yangtze River developed from a weak

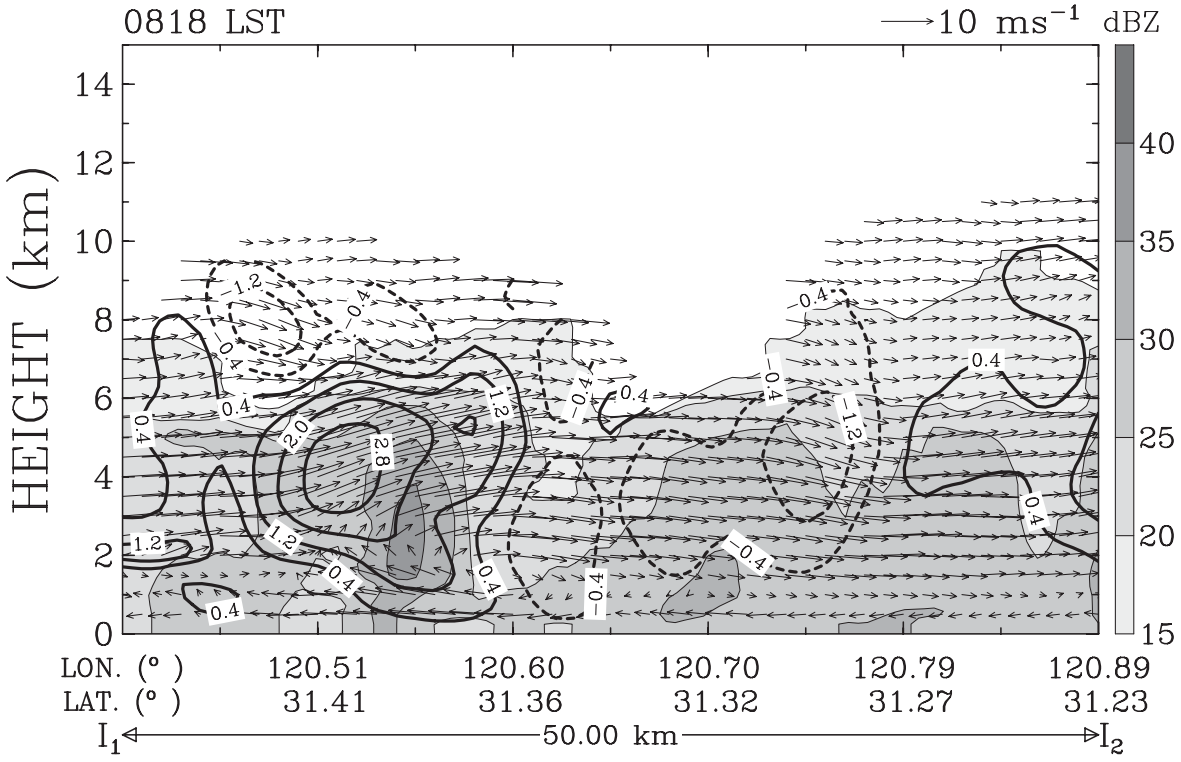

Fig. 21. Same as Fig. 18, except for 0818 LST 21 June 2002 and along line I_1I_2 in Fig. 20.

front with little convection into an intense one inducing the strong convective rainband along the front (Figs. 2, 5). The development of the front followed the increase in convergence both south and north of the front from 0200 LST (Fig. 5b). This implies that mesoscale frontogenesis would play an important role in the intensification of the front. To estimate the surface frontogenesis, following equation (Miller 1948) has been employed:

$$\frac{d}{dt}|\nabla\theta| = \frac{1}{|\nabla\theta|}\left\{-\left[\left(\frac{\partial\theta}{\partial x}\right)^2\frac{\partial u}{\partial x}+\left(\frac{\partial\theta}{\partial y}\right)^2\frac{\partial v}{\partial y}\right] - \left[\frac{\partial\theta}{\partial x}\frac{\partial\theta}{\partial y}\left(\frac{\partial v}{\partial x}+\frac{\partial u}{\partial y}\right)\right] - \left[\frac{\partial\theta}{\partial p}\left(\frac{\partial\theta}{\partial x}\frac{\partial\omega}{\partial x}+\frac{\partial\theta}{\partial y}\frac{\partial\omega}{\partial y}\right)\right] + \left[\frac{\partial\theta}{\partial x}\frac{\partial}{\partial x}\left(\frac{d\theta}{dt}\right)+\frac{\partial\theta}{\partial y}\frac{\partial}{\partial y}\left(\frac{d\theta}{dt}\right)\right]\right\} \quad (1)$$

where θ is the potential temperature; ω is the vertical p velocity; and u and v are the horizontal wind components. The first and second terms on the right-hand side represent stretching deformation and shear deformation, respectively. The sum of the first two terms represents the effect of horizontal deformation. The third and fourth terms represent the tilting and diabatic effects, respectively. Like previous studies (e.g., Chen and Li 1995), it is found that the major contributor to the surface frontogenesis was associated with horizontal deformation. It is also found that the magnitude of stretching deformation in this case was twice as much as that of shear deformation.

The distribution and evolution of the frontogenesis due to horizontal deformation at the surface is shown in Fig. 23. As expected, the frontogenesis along the front in the downstream region of the Yangtze River began to be enhanced from 0200 LST 21 June (Figs. 23c,d). It is well known that frontogenesis will produce a thermally direct circulation with the rising branch within warmer air and the sinking branch within colder air. Its rising branch will promote the development of convection. Consequently, the enhanced frontogenesis along the front from 0200 LST would account for

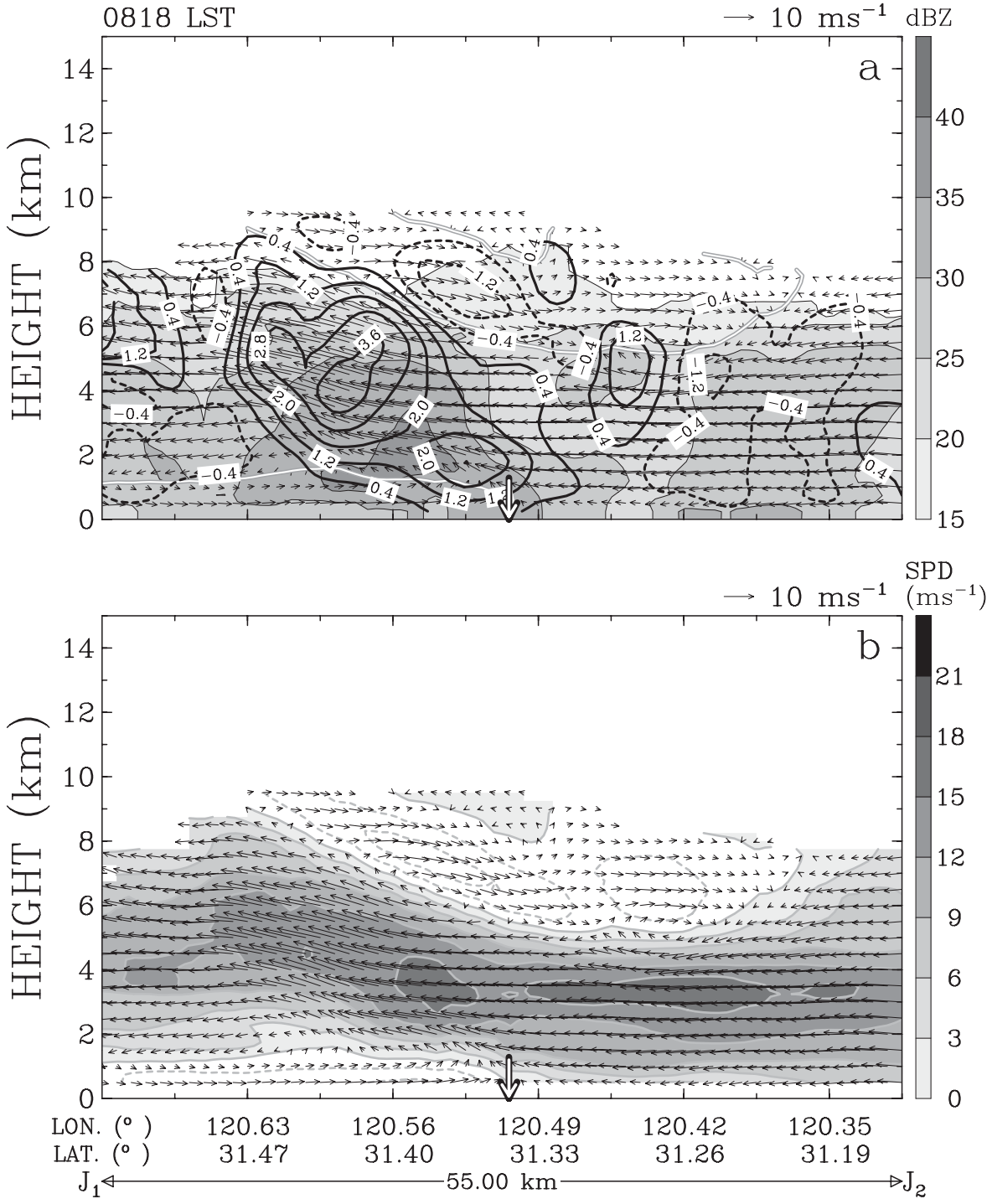

Fig. 22. Same as Fig. 19, except for 0818 LST 21 June 2002 and along line J_1J_2 in Fig. 20.

the activation of the front after 0500 LST when the rainband began to develop along the front (Figs. 23e,f).

At 0200 LST, it is noted that the intensification of convergence south of the front was associated with the divergence of low-level horizontal winds

caused by the topographic-enhanced convective system around (30°N, 118°E) (Figs. 5b, 23d). At the same time, the strongest convergence was found north of the front, which was responsible for the frontogenesis core around (33°N, 118.5°E). Note that enhanced convergence just north of the front was related to the intensification of low-level northeasterly winds north of the front. It was shown that the intensification and southward advancement of low-level northeasterly winds north of the front were related to the development of divergence further to the north around 34°N from 0200 LST (Fig. 5). Before this time, it is noted that some precipitation systems near 34°N were decaying with the lowest TBB of clouds keeping increase with time (Figs. 23a–c). Meanwhile, cooling of the surface air was observed in this region (Fig. 6). These facts suggest that the development of the divergence north of the front would be related to the evaporation of precipitation there. As indicated by Kato et al. (1995) and Geng and Yamada (2007), it is fairly common for precipitation systems to form and develop in some distances north of the Meiyu/Baiu front over the China Continent. The dryness of low-level air (see Figs. 2, 3) north of the front would provide more favorable environment for the subcloud evaporation of precipitation than wet conditions usually found south of and along the front. It appears that the development of the Meiyu/Baiu front through a regulation of precipitation systems north of the front would be a significant mesoscale process.

It was also shown from the Doppler radar observation that the frontal surface became deeper both in the eastern and western parts as the convection triggered by the front developed along the front (Figs. 13, 16, 19, 22). Especially, the front in the western part has developed much more deeply north of deeper and stronger convection. Many studies have investigated the impact of convective activities on the Meiyu/Baiu front over China. For example, Chen et al. (1998) found from numerical experiments that a Meiyu/Baiu front is weakened considerably in the absence of latent heating from convection along the front. Through potential vorticity diagnostic analysis, Chen et al. (2003) also indicated that latent heating by cumulus convection could further enhance the Meiyu/Baiu front. Like previous studies, such a positive feedback of convection to the development of a Meiyu/Baiu front could also be responsible for the further intensification of the front observed in the present case. The result of the present study further indicates that the distinct development of convective systems along the front would be important for creating a front with significant mesoscale along-frontal variation.

7.2 Distinct effects of the LLJ on the development of convective systems

As stated before, prefrontal environmental conditions of larger CAPE, smaller CIN, and lower LFC in the eastern part of the front imply that convection in this region could be stronger than that in the western part (Figs. 4). Nevertheless, both the upper-air observation and Doppler radar analysis showed the opposite result (Figs. 8, 9, 10–22). It was shown that a subsynoptic-scale LLJ formed south of the front (Figs. 3, 7). It appears that the distinct evolution of the LLJ would have a great impact on the variational development of convective systems along the front. The Doppler radar analysis showed that the intensity of the low-level cross-frontal flow south of the front was much weaker in the western part than that in the eastern part. This suggests the different orientation of the LLJ to the front in each part.

In the western part, the LLJ approached the front at a sharp angle (Fig. 24). This would be responsible for the weaker cross-frontal flow at low levels south of the front. It is noted that the primary convection moved southward together with the front and was always located just north of the front, which would allow it to be fed with low-level warm and moist air constantly. This situation apparently provided a favorable condition for convection and precipitation to develop strongly in the western part.

In the eastern part, on the other hand, the LLJ approached and overtook the front nearly at a right angle (Fig. 25). Although convective echoes formed near the front due to the lifting of low-level warm and moist air by the front, they soon moved far away from the front to the north and were followed by new convective echoes forming near the front. This would contribute to the northward extension of precipitation (Fig. 10) and the formation of multiple linear precipitation cores in the eastern part (Fig. 17). It is noted from Fig. 25 that the northward movement of convective echoes was quite similar to the speed of the northward penetration of the LLJ. This implies that the fast northward movement of convective echoes in the eastern part would be due to the steering by the LLJ. In the eastern part, as a convective cell forming near the

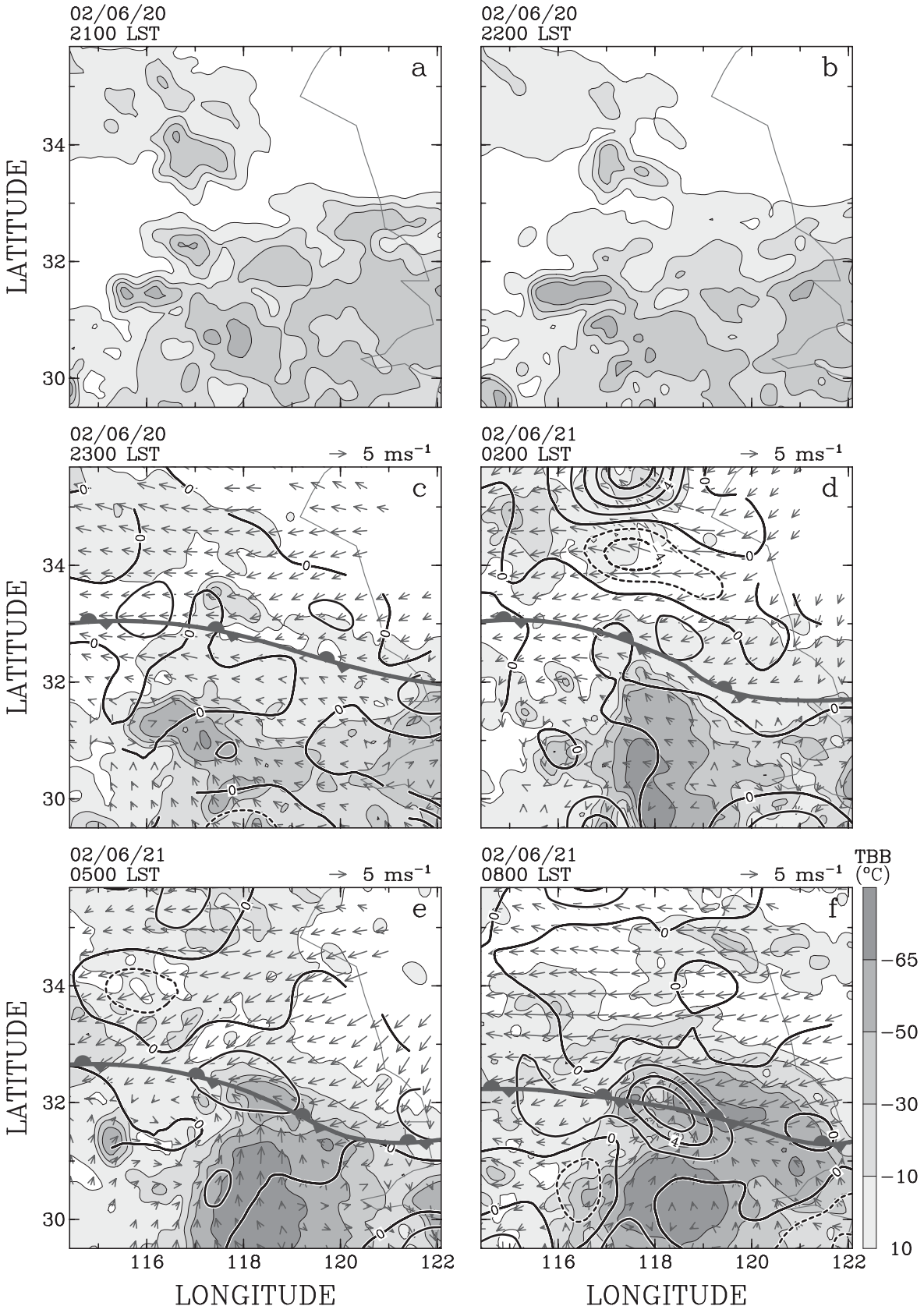
02/06/20
2100 LST
a
02/06/20
2200 LST
b
02/06/20
2300 LST
→ 5 ms⁻¹
c
02/06/21
0200 LST
→ 5 ms⁻¹
d
02/06/21
0500 LST
→ 5 ms⁻¹
e
02/06/21
0800 LST
→ 5 ms⁻¹
f
TBB
(°C)
−65
−50
−30
−10
10
LATITUDE
34
32
30
116
118
120
122
LONGITUDE

front soon moved north of the front with a new one being generated south of the old one, the old convective cell was soon cut off from the supplement of low-level warm and moist air and dominated by downdrafts at low levels (Fig. 19a). Consequently, this situation would have caused convection and precipitation in the eastern part to be weak.

It implies that the nearly parallel orientation of the LLJ to the front as seen in Fig. 24 would let the LLJ have a little effect on the movement of the convection relative to the front. On the other hand, the nearly normal orientation of the LLJ to the front as seen in Fig. 25 would let the LLJ exert strong impact on the movement of the convection away from the front. It appears that the normal orientation of the LLJ to the front would provide a favorable situation for the LLJ to overrun the front. Such an overrunning of the LLJ may be interpreted according to a theory viewing the balance between the horizontal vorticity of the environmental wind and the horizontal vorticity produced by the cold air at lower levels (e.g., Rotunno et al. 1988). Note that the normal orientation of the LLJ to the front causes the substantial cross-frontal component of the vertical shear below the jet maximum on the south side of the front (Fig. 19). In light of the theory of Rotunno et al. (1988), the strong prefrontal low-level flow would rapidly overrun the front after being lifted by the front, because it holds the considerable horizontal vorticity having the same sign as that created by the low-level cold air. It was shown that the LLJ was intensifying in the eastern part during the observation (Fig. 7). Although processes related to the intensification of the LLJ need further investigation, it seems that convective activities around the front (see Fig. 10) may play an important role (e.g., Nagata and Ogura 1991; Chen et al. 2006).

While the importance of the LLJ in the formation of heavy rainfall has been stressed by many previous studies (e.g., Ninomiya and Akiyama 1992), the present paper has shown that the LLJ would also play an opposite role when it orients at a nearly right angle to the Meiyu/Baiu front. It appears that the orientation of the LLJ to the Meiyu/Baiu front can be a supplementary measure that could make the tie of the LLJ to the heavy rainfall more precise. This study implies that the orientation of the LLJ to the front at a sharp angle is more favorable for the formation of strong convective systems along the Meiyu/Baiu front.

8. Summary and conclusions

The mesoscale structure and evolution of a Meiyu/Baiu front and precipitation along the front observed in the downstream region of the Yangtze River on 21 June 2002 have been analyzed by utilizing data from intensive observations of upper-air, surface, and five Doppler radars, as well as GMS IR and GANAL data. It is found that the front collocated with a large-scale wind shear line. The frontal zone was characterized by a subsynoptic-scale low-level jet (LLJ) to the south and the strong cross-frontal gradient of moisture. Meanwhile, a thermally direct circulation was observed ahead of the front and was centered in the middle troposphere. The prefrontal vertical circulation was toward the opposite direction of the vertical circulation associated with the front. It is found that the front evolved from an inactive front with little convection along it to an intensive one inducing a strong meso-α-scale rainband. The meso-α-scale rainband triggered by the front was composed of several meso-β-scale convective systems.

The activation of the front mainly followed an increase in the intensity of low-level east-northeasterly winds north of the front. The intensification of low-level east-northeasterly winds, which was associated with the development of the low-level divergence related to the evaporative cooling of precipitation systems located further to the north, would have helped to strengthen the low-level convergence and thermal contrast across the front, thus enhance the low-level frontogenesis along the front. Meanwhile, it appears that the latent heat release of convective systems developed along the front have exerted a positive feedback on the further development of the front. At the same time, distinct behaviors of the LLJ were found in the western and eastern parts of the downstream region of the Yangtze River. In the western part, the

Fig. 23. GMS infrared imageries (shaded) for (a) 2100 LST, (b) 2200 LST, (c) 2300 LST 20 June, (d) 0200 LST, (e) 0500 LST, and (f) 0800 LST 21 June 2002. In (c)–(d), distributions of the surface frontogenesis due to horizontal deformation (contoured every 2×10^{-10} K m^{-1} s^{-1}), surface horizontal winds (arrows), and the locations of the surface front are also shown.

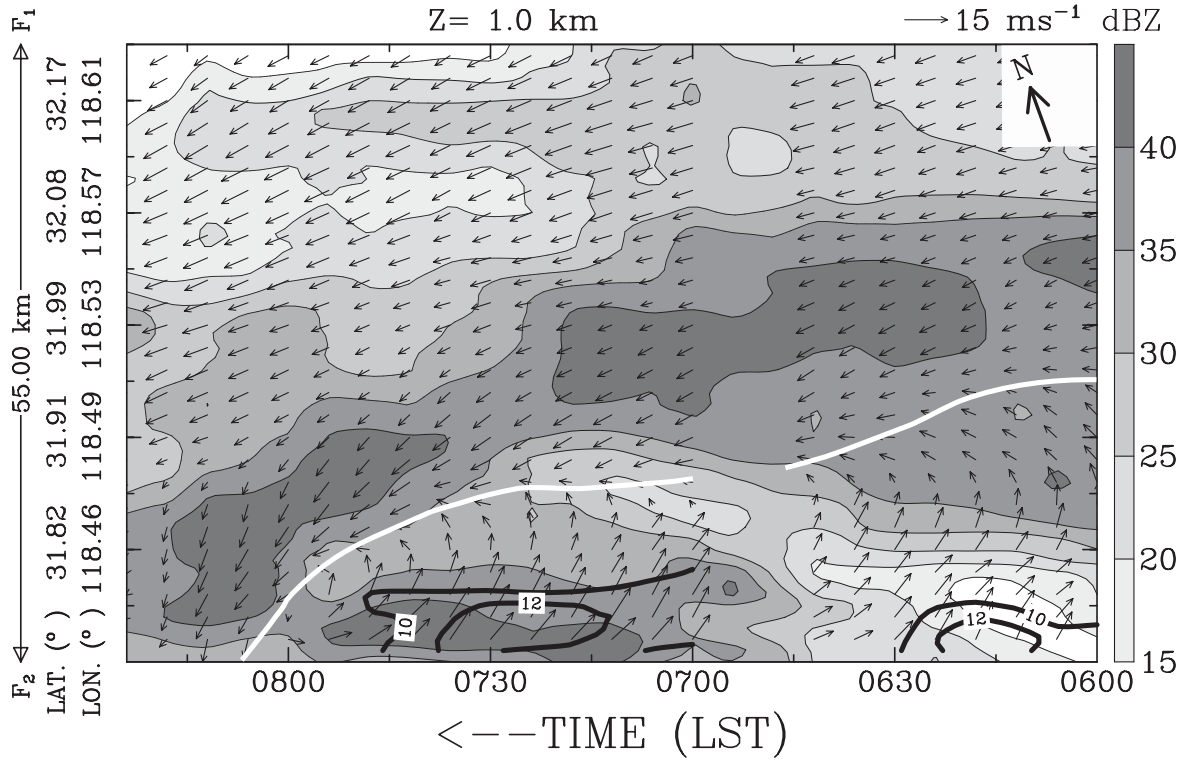

Fig. 24. Time-distance diagram of radar reflectivity (shaded), horizontal winds (arrows), and horizontal wind speeds (contoured every 2 m s^{-1} from 10 m s^{-1}) at the 1.0-km level along line F_1F_2 in Fig. 14. White line outlines the wind shear line associated with the front. Wind data at 0648 and 0654 LST were not available.

orientation of the LLJ to the front was at a sharp angle. In the eastern part, on the other hand, the LLJ oriented nearly normal to the front, overran the front at lower levels, and penetrated far to the north of the front.

Three-dimensional kinematic and reflectivity structures of two meso-β-scale convective systems, where one was in the western part and the other was in the eastern part, have been examined comprehensively from the Doppler radar analysis. In the western part, the meso-β-scale convective system evolved in a quasi-steady state. It was characterized by a deep and strong convective cell just north of the front and limited stratiform precipitation to the rear of the strong convective cell. In this region, the primary updraft triggered by the front sloped largely northward in the lower troposphere and became nearly upright and strong from the middle troposphere. On the other hand, the meso-β-scale convective system in the eastern part was featured by multiple shallow and weak convective cells across the front and extended stratiform precipitation both south and north of convective cells. In this region, a convective cell that was generated near the front soon moved northward and became decaying to the north of the front. A new convective cell repeatedly formed near the front after the old one moved away.

It appears that distinct behaviors of the LLJ would have greatly affected the convective organization along the front. In the western part, the sharp orientation of the LLJ to the front would allow the convection triggered by the front to be attached to the front and to be fed with warm and moist air constantly. These processes would account for the generation of narrow and consolidated meso-β-scale convective systems in the western part. In the eastern part, on the other hand, the overrun of the LLJ to the north of the surface front would force the convection triggered by the front to move fast away from the front and to be cut off soon from prefrontal low-level warm and moist air. These processes would be responsible for the formation of weak, wide and loosely organized

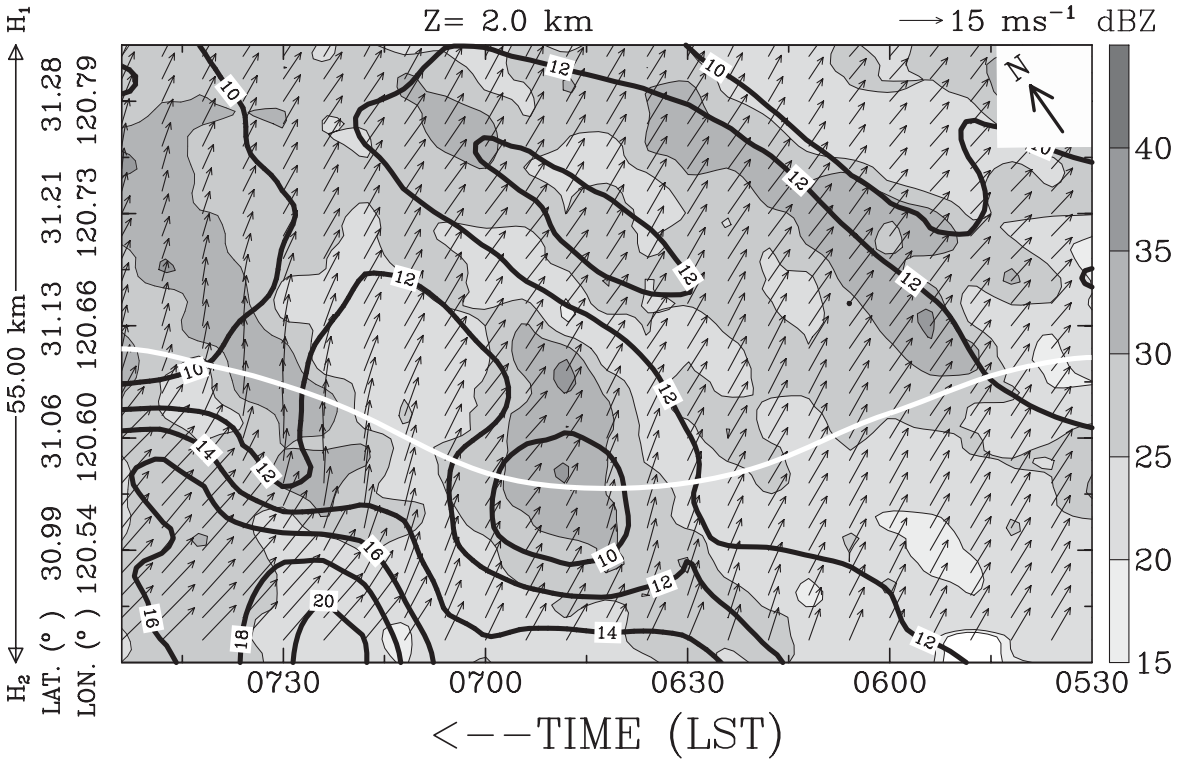

Fig. 25. Time-distance diagram of radar reflectivity (shaded), horizontal winds (arrows), and horizontal wind speeds (contoured every 2 m s^{-1} from 10 m s^{-1}) at the 2.0-km level along line H_1H_2 in Fig. 17. White line outlines the wind shear line associated with the front at the 0.5-km level.

meso-β-scale convective systems in the eastern part.

This study has shown that the evolution of the frontal zone and convective systems along a Meiyu/Baiu front can be significantly distinct in the downstream region of the Yangtze River. It appears that the mesoscale along-frontal variability of the Meiyu/Baiu frontal zone can be one of significant factors affecting modes of convective organization and determining where deep convection (thus heavy rainfall) would occur along the front in a limited distance.

Acknowledgements

The authors wish to express their appreciation to all members involved in the intensive observation conducted in the downstream region of the Yangtze River. We are very grateful to Prof. Y. Ni and Prof. L. Liu of the Chinese Academy of Meteorological Sciences for collecting observational data. Special thanks go to Dr. K. Tsuboki, Dr. T. Shinoda, and Mr. Minda of Nagoya University, Dr. M. Kawashima, and Mr. M. Ooi of Hokkaido University for supporting the Doppler radar observation. We would also like to thank Kochi University for providing GMS data.

References

Akiyama, T., 1989: Large, synoptic and meso scale variations of the Baiu front, during July 1982. Part I: Cloud features. *J. Meteor. Soc. Japan*, **67**, 57–81.

Akiyama, T., 1990: Large, synoptic and mesoscale variations of the Baiu front, during July 1982. Part II: Frontal structure and disturbances. *J. Meteor. Soc. Japan*, **68**, 557–574.

Barnes S. L., 1964: A technique for maximizing details in a numerical weather map analysis. *J. Appl. Meteor.*, **3**, 396–409.

Biggerstaff, M. I., and R. A. Houze, Jr., 1991: Kinematic and precipitation structure of the 10–11 June 1985 squall line. *Mon. Wea. Rev.*, **119**, 3034–3065.

Chen, G. T. J., and C. P. Chang, 1980: The structure and vorticity budget of an early summer monsoon trough (Mei-Yu) over southeastern China and Japan. *Mon. Wea. Rev.*, **108**, 942–953.

Chen, G. T. J., C. C. Wang, and S. C. S. Liu, 2003: Potential vorticity diagnostics of a Mei-Yu front case. *Mon. Wea. Rev.*, **131**, 2680–2696.

Chen, G. T. J., 2004: Research on the phenomena of Meiyu during the past quarter century: An overview. World Scientific Series for Meteorology of East Asia Vol. 2, East Asian Monsoon, C. P. Chang, Ed., *World Scientific Publishing Co.*, 357–403.

Chen, G. T. J., C. C. Wang, and L. F. Lin, 2006: A diagnostic study of a retreating Mei-Yu front and the accompanying low-level jet formation and intensification. *Mon. Wea. Rev.*, **134**, 874–896.

Chen, S. J., Y. H. Kuo, W. Wang, Z. Y. Tao, and B. Cui, 1998: A modeling case study of heavy rainstorms along the Mei-Yu front. *Mon. Wea. Rev.*, **126**, 2330–2351.

Chen, Y. L., Y. X. Zhang, and N. B. F. Hui, 1989: Analysis of a surface front during the early summer rainy season over Taiwan. *Mon. Wea. Rev.*, **117**, 909–931.

Chen, Y. L., and N. B. F. Hui, 1990: Analysis of a shallow front during Taiwan Area Mesoscale Experiment. *Mon. Wea. Rev.*, **118**, 2649–2667.

Chen, Y. L., and N. B. F. Hui, 1992: Analysis of a relatively dry front during the Taiwan area mesoscale experiment. *Mon. Wea. Rev.*, **120**, 2442–2468.

Chen, Y. L., and J. Li, 1995: Large-scale conditions favorable for the development of heavy rainfall during TAMEX IOP 3. *Mon. Wea. Rev.*, **123**, 2978–3002.

Cressman, G. P., 1959: An operational objective analysis system. *Mon. Wea. Rev.*, **87**, 367–374.

Ding, Y. H., 1992: Summer monsoon rainfalls in China. *J. Meteor. Soc. Japan*, **70**, 373–396.

Gao, J., M. Xue, A. Shapiro, and K. K. Droegemeier, 1999: A variational method for the analysis of three-dimensional wind fields form two Doppler radars. *Mon. Wea. Rev.*, **127**, 2128–2142.

Geng, B., H. Yamada, K. K. Reddy, H. Uyeda, and Y. Fujiyoshi, 2004: An observational study of the development of a rainband on a Meiyu front causing heavy rainfall in the downstream region of the Yangtze River. *J. Meteor. Soc. Japan*, **82**, 1095–1115.

Geng, B., and H. Yamada, 2007: Diurnal variations of the Meiyu/Baiu rain belt. *SOLA*, **3**, 61–64.

Ishihara, M., Y. Fujiyoshi, A. Tabata, H. Sakakibara, K. Akaeda, and H. Okamura, 1995: Dual Doppler radar analysis of an intense mesoscale rainband generated along the Baiu front in 1988: Its kinematical structure and maintenance process. *J. Meteor. Soc. Japan*, **73**, 139–163.

Jorgensen, D. P., and M. A. LeMone, 1989: Vertical velocity characteristics of oceanic convection. *J. Atmos. Sci.*, **46**, 621–640.

Jorgensen, D. P., M. A. LeMone, and B. J. D. Jou, 1991: Precipitation and kinematic structure of an oceanic mesoscale convective system. Part I: Convective line structure. *Mon. Wea. Rev.*, **119**, 2608–2637.

Kato, K., 1985: On the Abrupt Change in the Structure of the Baiu Front Over the China Continent in Late May of 1979. *J. Meteor. Soc. Japan*, **63**, 20–36.

Kato, K., J. Matsumoto, and H. Iwasaki, 1995: Diurnal variation of Cb-Clusters over China and its relation to large-scale conditions in the summer of 1979. *J. Meteor. Soc. Japan*, **73**, 1219–1234.

Kim, H. W., and D. K. Lee, 2006: An observational study of mesoscale convective systems with heavy rainfall over the Korean Peninsula. *Wea. Forecasting*, **21**, 125–148.

Li, J., Y. L. Chen, and W. C. Lee, 1997: Analysis of a heavy rainfall event during TAMEX. *Mon. Wea. Rev.*, **125**, 1060–1082.

Lin, Y. J., R. W. Pasken, and H. W. Chang, 1992: The structure of a subtropical prefrontal convective rainband. Part I: Mesoscale kinematic structure determined from dual-Doppler measurements. *Mon. Wea. Rev.*, **120**, 1816–1836.

Lucas, C., E. J. Zipser, and M. A. LeMone, 1994: Vertical velocity in oceanic convection off tropical Australia. *J. Atmos. Sci.*, **51**, 3182–3193.

Matsumoto, S., K. Ninomiya, and S. Yoshizumi, 1971: Characteristic features of Baiu front associated with heavy rainfall. *J. Meteor. Soc. Japan*, **49**, 267–281.

Miller, J. E., 1948: On the concept of frontogenesis. *J. Meteor.*, **9**, 169–171.

Moteki, Q., H. Uyeda, T. Maesaka, T. Shinoda, M. Yoshizaki, and T. Kato, 2004: Structure and development of two merged rainbands observed over the East China Sea during X-BAIU-99. Part I: meso-β-scale structure and development processes. *J. Meteor. Soc. Japan*, **82**, 19–44.

Ninomiya, K., and T. Akiyama, 1974: Band structure of mesoscale echo cluster associated with low-level jet stream. *J. Meteor. Soc. Japan*, **52**, 300–313.

Ninomiya, K., and H. Muraki, 1986: Large-scale circulations over east Asia during Baiu period of 1979. *J. Meteor. Soc. Japan*, **64**, 409–429.

Ninomiya, K., and T. Akiyama, 1992: Multi-scale features of Baiu, the summer monsoon over Japan and the East Asia. *J. Meteor. Soc. Japan*, **70**, 467–495.

Ninomiya, 2000: Large- and meso-α-scale characteristics of Meiyu/Baiu front associated with intense rainfalls in 1–10 July 1991. *J. Meteor. Soc. Japan*, **78**, 141–157.

O'Brien, J. J., 1970: Alternative solution to the classical vertical velocity problem. *J. Appl. Meteor.*, **9**, 197–203.

Ogura, Y., T. Asai, and K. Dohi, 1985: A case study of a heavy precipitation event along the Baiu front in northern Kyushu, 23 July 1982: Nagasaki heavy rainfall. *J. Meteor. Soc. Japan*, **62**, 883–900.

Orlanski, I., 1975: A rational subdivision of scales for atmospheric processes. *Bull. Amer. Meteor. Soc.*, **56**, 527–530.

Ray, P. S., C. L. Ziegler, W. Bumgarner, and R. J. Serafin, 1980: Single and multiple-Doppler radar observations of tornadic storms. *Mon. Wea. Rev.*, **108**, 1607–1625.

Ray, P. S., A. Robinson, and Y. Lin, 1991: Radar analysis of a TAMEX frontal System. *Mon. Wea. Rev.*, **119**, 2519–2539.

Rotunno, R., J. B. Klemp, and M. L. Weisman, 1988: A theory for strong, long-lived squall lines *J. Atmos. Sci.*, **45**, 463–485.

Shimizu, S., and T. Maesaka, 2007: Multiple Doppler radar analysis using variational technique to retrieve three-dimensional wind field. Report of the National Research Institute for Earth Science and Disaster Prevention, **70**, 1–8 (in Japanese).

Takahashi, N., H. Uyeda, K. Kikuchi, and K. Iwanami, 1996: Mesoscale and convective scale features of heavy rainfall events in late period of the Baiu season in July 1988, Nagasaki Prefecture. *J. Meteor. Soc. Japan*, **74**, 539–561.

Trier, S. B., D. B. Parsons, and T. J. Matejka, 1990: Observations of a subtropical cold front in a region of complex terrain. *Mon. Wea. Rev.*, **118**, 2449–2470.

Xu, K. M., and D. A. Randall, 2001: Updraft and downdraft statistics of simulated tropical and midlatitude cumulus convection. *J. Atmos. Sci.*, 1630–1649.

Yamada, H., B. Geng, K. K. Reddy, H. Uyeda, and Y. Fujiyoshi, 2003: Three-dimensional structure of a mesoscale convective system in a Baiu-frontal depression generated in the downstream region of the Yangtze River. *J. Meteor. Soc. Japan*, **81**, 1243–1271.

Zipser, E. J., and M. A. LeMone, 1980: Cumulonimbus vertical velocity events in GATE. Part II: Synthesis and model core structure. *J. Atmos. Sci.*, **37**, 2458–2469.